CHAPTER 4

Enzymology:

4.1 Introduction:

4.1.1 Enzyme kinetics:

According to Garrett & Grisham (2002), kinetics is the branch of science concerned with the rates of chemical reactions and enzyme kinetics is the study of the biological roles of the enzymatic catalysts. Enzyme kinetics attempt to determine the maximum reaction velocity that the enzyme can attain and its binding affinity for given substrates and inhibitors. Analyzing the enzymatic rate under different conditions can provide insights into the enzyme's mechanism of catalytic action and an understanding of overall metabolism.

Enzyme kinetics is important in the determination of the affinity of an inhibitor for the enzyme. The affinity of an inhibitor for the enzyme is a measure of the degree to which an inhibitor inhibits the enzyme. The inhibitor's potency is expressed by the K_i value, also known as the inhibitor constant. The general equation for the chemical reaction between a substrate and an enzyme can be illustrated as:

$$S + E \overset{v_i}{\rightarrow} SE$$

Where S is the substrate and E is the enzyme. v_i represents the initial velocity of the forward reaction. The velocity or rate of the reaction can be expressed as the amount of substrate S consumed over time, or the amount of the substrate enzyme complex formed over time. At low concentrations of the substrate S, v is proportional to [S], as expected for a first order reaction. However, as [S] continues to increase, the enzyme becomes saturated and v becomes virtually independent of S and it approaches a maximal limit (V_{max}). Because the rate is no longer dependent on [S] at these high concentrations, the enzyme now follows zero order kinetics. At this point every enzyme molecule in the reaction has its substrate binding site occupied by S (Garrett & Grisham, 2002).

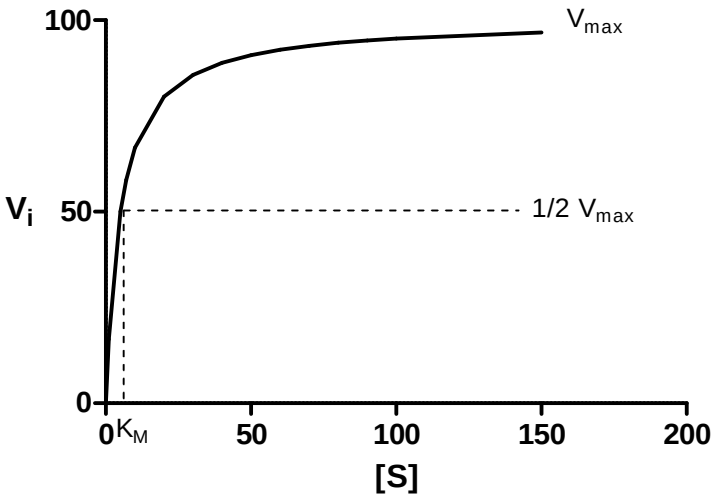

Figure 4.1.1 A graph showing the relationship between V_{max} and K_m

The Michaelis-Menten equation:

The Michaelis-Menten equation describes the relationship between the initial velocity (v_i) and the concentration of the substrate ([S]).

$$v_i = \frac{V_{max}[S]}{K_m + [S]}$$

This equation predicts that the rate of an enzyme-catalyzed reaction, v_i, is at any moment determined by two constants, K_m and V_{max}, and the concentration of the substrate at that moment. V_{max} is the maximal velocity that is experienced as the enzyme becomes saturated and the Michaelis constant (K_m), is the concentration of the substrate S that leads to half-maximal velocity (Garrett & Grisham, 2002).

The Michaelis-Menten equation can be evaluated under three conditions namely:

1) When [S] is much less than K_m, then K_m + [S] can be set equal to K_m

$$v_i = \frac{V_{max}[S]}{K_m}$$

2) When [S] is greater K_m, then K_m + [S] can be set equal to [S]

$$v_i = V_{max}$$

3) When [S] equals K_m, v_i can be set equal to $V_{max}/2$

$$v_i = \frac{V_{max}}{2}$$

The Lineweaver-Burk plot:

Due to the hyperbolic shape of the v versus [S] plots, V_{max} can only be determined by the asymptotic approach of v to some limiting value as [S] increased indefinitely. This created a need for the Michaelis-Menten equation to be adapted to a straight line equation. The best known of these straight line equations is the Lineweaver-Burk double-reciprocal plot. Taking the reciprocal of both sides of the Michaelis-Menten equation and arranging it in the form y = mx + c gives the following equation:

$$\frac{1}{V} = \left(\frac{K_m}{V_{max}}\right)\left(\frac{1}{[S]}\right) + \frac{1}{V_{max}}$$

Plotting 1/v versus 1/[S] gives a straight line with an x-intercept of $-1/K_m$, a y-intercept of $1/V_{max}$ and a slope of K_m/V_{max}. Both K_m and V_{max} can be estimated accurately by the extrapolation of the straight line (Garrett & Grisham, 2002).

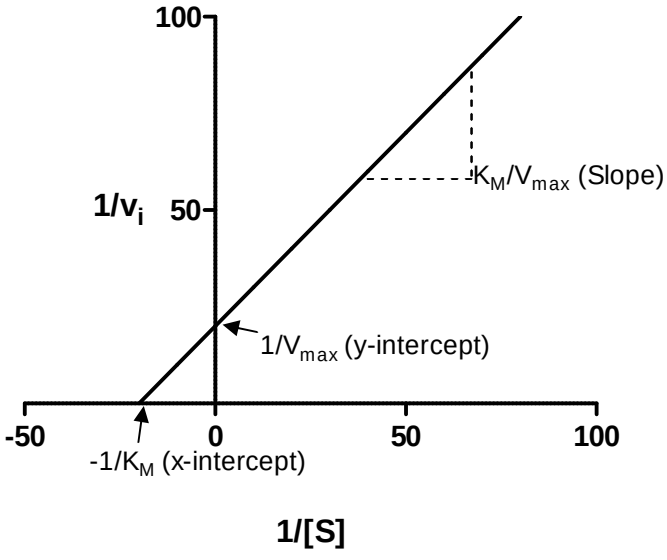

Figure 4.1.2 An example of a Lineweaver-Burk plot.

During competitive inhibition of an enzyme, an inhibitor (I) binds reversibly to the enzyme at the same site as the substrate S. The binding of the inhibitor and substrate is mutually exclusive and a competitive process. It is physically impossible for the substrate and the

inhibitor to be bound to the enzyme at the same time. The substrate and inhibitor often share a high degree of similarity because they bind to the same site on the enzyme.

The adapted Michaelis-Menten equation for the rate of an enzymatic reaction in the presence of a fixed concentration of the competitive inhibitor [I] is:

$$v = \frac{V_{max}[S]}{[S] + K_m\left(1 + \frac{[I]}{K_i}\right)}$$

The equilibrium constant, K_i, is a dissociation constant for the breakdown of the EI complex. The smaller the K_i value for I, the more potent the inhibitor. The K_m term in the denominator is increased by the factor (1+ [I]/K_i). This relationship predicts that v is lower in the presence of the inhibitor. From the Lineweaver-Burk plot for competitive inhibition the following observations can be made: at a given [I], 1/v increases, therefore v decreases; when [S] becomes infinite v = V_{max} because all the enzyme is in the ES form and it is therefore unaffected by [I]; the value of the –x-intercept decreases as [I] increases. The x-intercept is often referred to as the apparent K_m, because it is the K_m apparent under these conditions. All the lines share a common y-intercept because V_{max} is unaffected by I. K_i can be determined by calculating the K_m value in the absence and presence of the inhibitor and using the following equation for the x-intercept (Garrett & Grisham, 2002):

$$x = \frac{-1}{K_m}\left(1 + \frac{[I]}{K_i}\right)$$

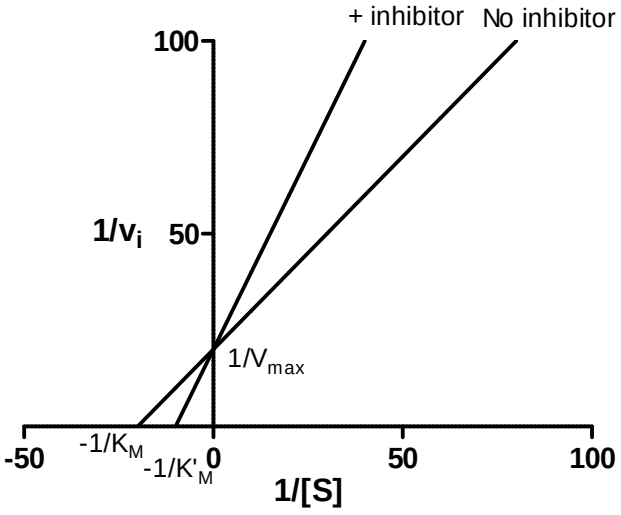

Figure 4.1.3 Lineweaver-Burk plots illustrating competitive inhibition.

The IC_{50} value:

The IC_{50} value is the inhibitor concentration that produces 50% enzyme inhibition in the presence of a substrate. Inhibitors with small IC_{50} values are therefore considered to be more potent inhibitors with high binding affinities for the enzyme active site.

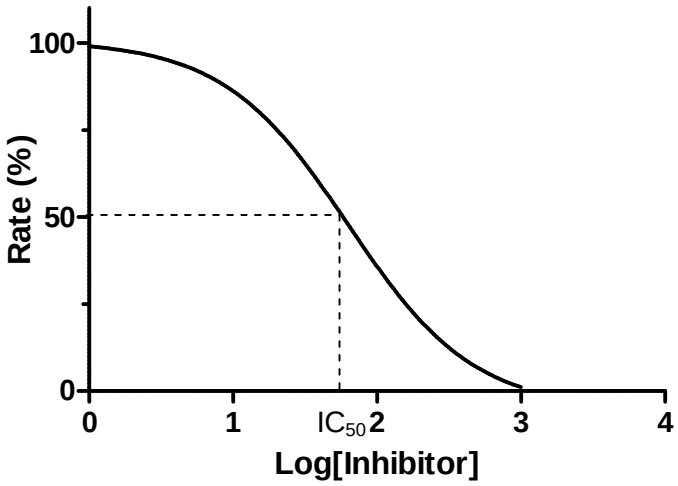

Figure 4.1.4 Graphical representation of the IC_{50} value.

The relationship between IC_{50} and K_i is indicated by the following equation (Silverman, 2004):

$$IC_{50} = \left(1 + \frac{[S]}{K_m}\right) K_i$$

4.1.2 Overview of this chapter:

In this chapter selected drugs that were found to map to the *structure-based* pharmacophore models of MAO-A and MAO-B will be evaluated as *in vitro* inhibitors of the MAO enzymes. Not all of the hits will be evaluated as *in vitro* inhibitors and only a subset will be selected for screening. The selection of the compounds to be screened was based on the commercial availability of the compounds and cost. Drugs that are not readily commercially available and of high cost were not evaluated. The Fit-Values for the MAO-A and MAO-B pharmacophore models were also considered when selecting compounds for *in vitro* evaluation. Compounds with high Fit-Values were preferred to those with lower Fit-Values. In total 26 compounds were selected for *in vitro* analysis.

The following *in vitro* bioassays will be carried out in this chapter:

- Determination of the IC_{50} values for the inhibition of MAO-A and MAO-B. For this purpose sigmoidal concentration-inhibition curves will be constructed. These experiments will be conducted for all test drugs.
- The reversibility of the inhibition of MAO-A and MAO-B by two selected inhibitors (pentamidine and phenformin) will be examined. For this purpose the recovery of enzyme activity after dilution of the enzyme-inhibitor complexes will be evaluated.
- For two selected inhibitors (pentamidine and phenformin) the reversibility of inhibition of MAO-A and MAO-B will be examined by performing dialysis of enzyme-inhibitor complexes.
- To determine if the active inhibitors are competitive inhibitors, Lineweaver-Burk plots will be constructed. These studies will be conducted for a selected inhibitor (pentamidine).

In addition, for those drugs that proved to be particularly interesting inhibitors of MAO-A and/or MAO-B, the docked orientations in MAO-A and/or MAO-B will be presented and their interactions with the active sites of the enzymes will be analyzed. The drugs selected for this purpose are pentamidine and phenformin. The orientations of these drugs within the *structure-based* pharmacophore models will also be presented.

In this chapter the methods that were used will be firstly discussed. This will be followed by the results (dose-response curves) for those drugs that mapped to the *structure-based* pharmacophore models of MAO-A and MAO-B, but proved not to be inhibitors of MAO-A or MAO-B. The results (dose-response curves and results of reversibility studies) of those drugs that were found to be MAO-A or MAO-B inhibitors will subsequently be given. As mentioned above, for selected inhibitors, the results of the dialysis studies and Lineweaver-

Burk plots will also be presented. This chapter will also compare the MAO-A and MAO-B inhibitory potencies of known MAO inhibitors with the potencies of the drugs that were found to be MAO-A or MAO-B inhibitors. The known inhibitors selected for this purpose are:

- Toloxatone, a MAO-A inhibitor
- Lazabemide, a MAO-B inhibitor

The subsequent chapter (Chapter 5) will be presented as an article, which discusses the MAO inhibitory properties of selected drugs that were found to be significant MAO inhibitors. The purpose of this article is to evaluate the probability of these drugs to exhibit MAO inhibition in the clinical setting. In addition, the article will also demonstrate that the results of this study are publishable. Based on their promising or interesting MAO inhibitory potencies, the MAO inhibitory properties of the following drugs will be presented in a concept article:

- pentamidine
- phenformin

It should be noted that for pentamidine and phenformin, the MAO inhibition data will be presented in this Chapter as well as in the subsequent article. Although this will result in some redundancy, this method of presentation will facilitate the detailed discussion of the inhibition data in the articles and prevent ambiguity.

4.1.3 Enzymology:

There are several methods available to test MAO-activity *in vitro*. A fluorometric assay was used to determine the IC_{50} values of the inhibitors in this study. Kynuramine was used as a substrate because it displays similar K_m values towards the two enzymes with values of 16.1 µM and 22.7 µM for MAO-A and MAO-B, respectively (Legoabe *et al.*, 2011). The assay is based on the measurement of the extent by which an inhibitor reduces the MAO-catalyzed oxidation of kynuramine to the fluorescent product, 4-hydroxyquinoline in basic solutions. The concentrations of 4-hydroxyquinoline were measured fluorometrically at an excitation wavelength of 310 nm and an emission wavelength of 400 nm.

Inhibitors may be classified as reversible or irreversible inhibitors. As mentioned above, to evaluate the reversibility of enzyme inhibition, recovery of enzyme activity after dilution of the

enzyme-inhibitor complexes will be examined. In addition, dialysis of enzyme-inhibitor complexes will be also be performed.

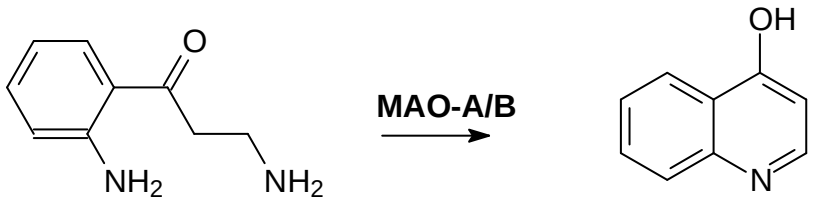

Kynuramine **4-hydroxyquinoline**

Figure 4.1.5 The oxidative deamination of kynuramine by MAO-A or MAO-B to yield 4-hydroxyquinoline.

4.2 Chemicals and instrumentation:

A Varian Cary Eclipse fluorescence spectrophotometer was used for the fluorometric measurements. Insect cell microsomes containing recombinant human MAO-A and MAO-B (5 mg/ml), kynuramine.2HBr, (*R*)-deprenyl HCl, pargyline HCl and the test drugs were obtained from Sigma-Aldrich. The Graphpad Prism® 5 software package was used to construct sigmoidal dose-response curves and to determine the IC_{50} values.

4.3 Determining the IC_{50} values

In this study, IC_{50} values were determined in order to express the potencies by which the active drugs inhibit MAO-A and MAO-B.

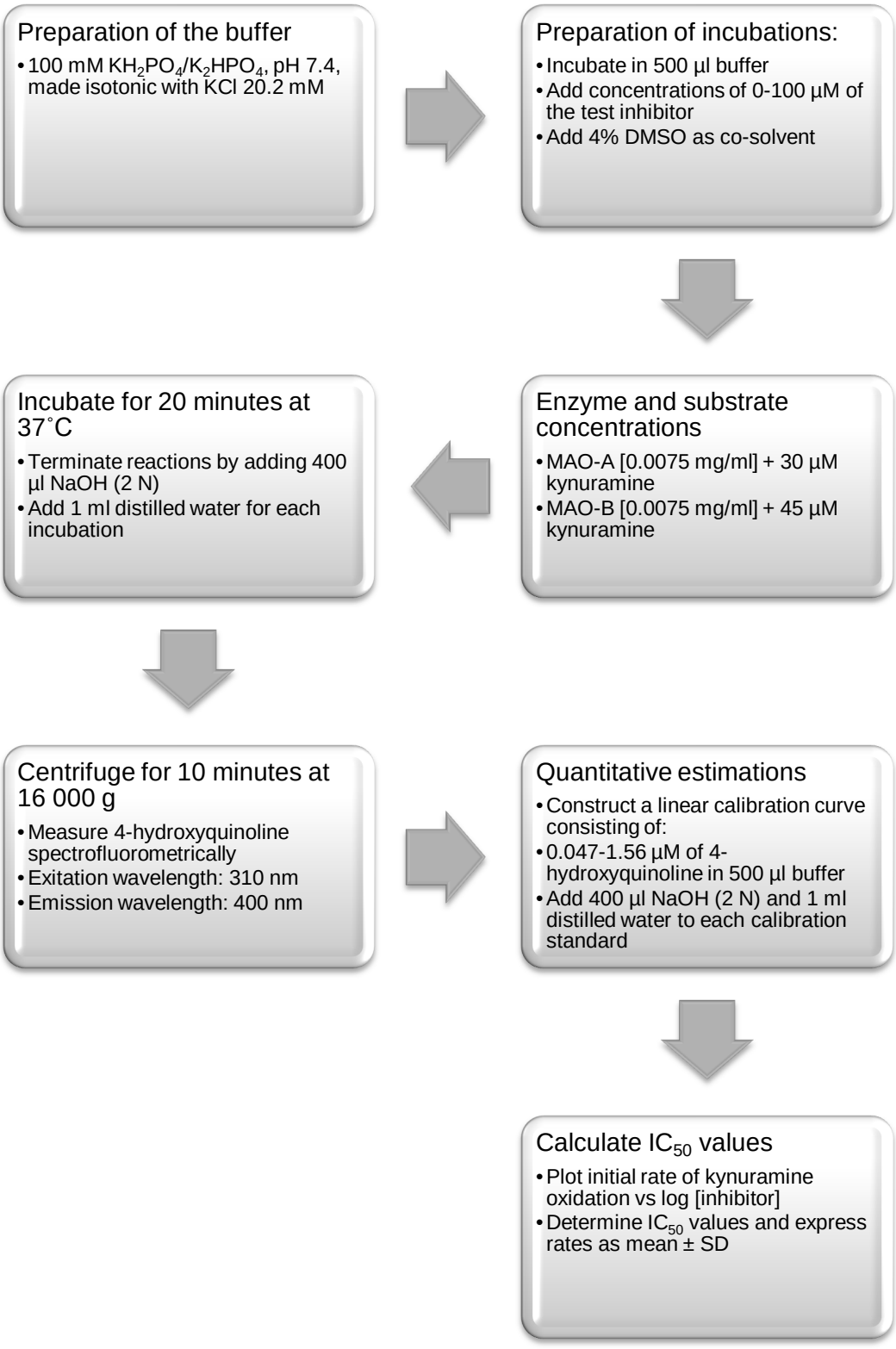

Figure 4.3.1 Diagrammatic representation of the method for determining IC_{50} values for the inhibition of MAO-A and MAO-B.

4.3.1 Method (see figure 4.3.1 for diagrammatic overview):

- Microsomal preparations of insect cells containing recombinant human MAO-A (5 mg/ml) and human MAO-B (5 mg/ml) were obtained from Sigma-Aldrich and were pre-aliquoted and stored at -70 ˚C. The incubations contained the following for the purpose of the IC_{50} value determinations:

    - 500 µl potassium phospate buffer (100 mM, pH 7.4, made isotonic with KCl)
    - MAO-A (0.0075 mg/ml) or MAO-B (0.0075 mg/ml)
    - Various concentrations of the test inhibitor (0-100 µM)
    - 4% DMSO co-solvent
    - Kynuramine as a substrate. The final concentrations of the kynuramine substrate were 30 µM for MAO-A and 45 µM for MAO-B.

- These reactions were incubated for 20 minutes at 37 ˚C, after which they were terminated by the addition of 400 µl NaOH. Distilled water (1 ml) was added to each reaction. The reactions were then centrifuged for 10 minutes at 16 000 g.
- The concentration of 4-hydroxyquinoline in each incubation was determined spectrofluorometrically by measuring the fluorescence of the supernatant at an excitation wavelength of 310 nm and an emission wavelength of 400 nm. The PMT voltage of the spectrofluorometer was set to medium with excitation and an emission slit widths of 5 mm and 10 mm, respectively, for MAO-B. For MAO-A, the PMT voltage was set to low with an excitation slit width of 10 mm and an emission slit of 20 mm.

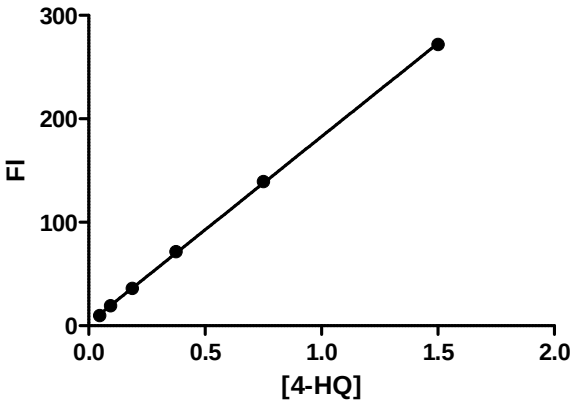

Figure 4.3.2 An example of the calibration curves routinely obtained in this study. The graph is that of fluorescence intensity (FI) of 4-hydroxyquinoline versus the concentration of authentic 4-hydroxyquinoline (4-HQ) in micromolar.

- Quantitative estimations were made by using a linear calibration curve, which was constructed with known amounts (0.047 – 1.56 µM) of 4-hydroxyquinoline dissolved in 500 µl potassium phosphate buffer (100 mM, pH 7.4, made isotonic with KCl 20.2 mM). Volumes of 400 µl NaOH (2 N) and 1000 µl water were added to each calibration standard. Control samples were added to confirm that the test inhibitors do not fluorescence or reduce the fluorescence of 4-hydroxyquinoline under the conditions used in the assay. The fluorescence values obtained in the inhibition studies should fall within the range of the calibration curve, which should display a high degree of linearity.

- The MAO catalytic rates were calculated from the endpoint concentration of 4-hydroxyquinoline (nM) in the supernatants, the incubation time (20 min) and the enzyme concentration (0.0075 mg protein/ml), and were expressed as nmol 4-hydroxyquinoline formed/min.mg protein.

- In order to determine an IC_{50} value, the initial rate of MAO catalysis was graphically plotted against the logarithm of the inhibitor concentration in order to obtain a sigmoidal dose-response curve. Each sigmoidal curve consisted of at least 6 different inhibitor concentrations spanning 3 orders of magnitude. GraphPad Prism® 5 was used to fit the inhibition date to the one site competition model. The IC_{50} values were determined in triplicate and expressed as mean ± standard deviation (SD).

4.4 Recovery of enzyme activity after dilution studies:

- For this study, kynuramine served as a substrate. All incubations were conducted in potassium phosphate buffer (100 mM, pH 7.4, made isotonic with KCl 20.2 mM). DMSO (4%) was added to each reaction as a co-solvent.
- Human recombinant MAO-A and MAO-B were pre-incubated with the selected inhibitor for 30 minutes at 37 ˚C. The concentration of the enzymes used were 0.75 mg/ml for MAO-A and MAO-B and the inhibitor concentrations were equal to 10-fold and 100-fold the measured IC_{50} values for the inhibition of MAO-A and MAO-B, respectively.
- As negative control, the MAO enzymes were also incubated in the absence of inhibitor. The irreversible MAO inhibitors pargyline (for MAO-A) and (*R*)-deprenyl (for MAO-B) were used as positive control inhibitors at concentrations of 10-fold their IC_{50} values.
- 50 µl of the enzyme and inhibitor mixture was subsequently diluted 100-fold with the addition of kynuramine to yield final concentrations of the test compound of 0.1 x IC_{50} and 1 x IC_{50}. The pargyline and (*R*)-deprenyl containing mixtures were similarly diluted to yield final concentrations of these inhibitors of 0.1 x IC_{50}. The final enzyme concentration was 0.0075 mg/ml and the final kynuramine concentrations were 45 µM for MAO-A and 30 µM for MAO-B, respectively.
- The reactions were then incubated at 37 ˚C for a period of 20 min and were subsequently terminated by the addition of 400 µl NaOH (2 N) and 1 ml distilled water. The mixtures were then centrifuged for 10 minutes at 16 000 g.
- The concentrations of the 4-hydroxyquinoline generated by MAO were measured spectrofluorometrically as described in paragraph 4.3.1. The experiments were carried out in triplicate and a calibration curve was prepared for each data set. The calibration curve was constructed with known amounts (0.047 – 1.56 µM) of 4-hydroxyquinoline dissolved in 500 µl potassium phosphate buffer (100 mM, pH 7.4, made isotonic with KCl 20.2 mM). Volumes of 400 µl NaOH (2 N) and 1 ml water were added to each calibration standard.

The purpose of the dilution studies is to determine whether the inhibitor acts as a reversible inhibitor or as a time-dependent inactivator of human MAO-A and MAO-B. This was achieved by constructing a histogram to determine whether enzyme activity is recovered when the enzyme-inhibitor complex is diluted. The MAO activities recorded in presence of

the test inhibitors were compared to the MAO activities recorded in presence the known time-dependent inactivators, (*R*)-deprenyl and pargyline.

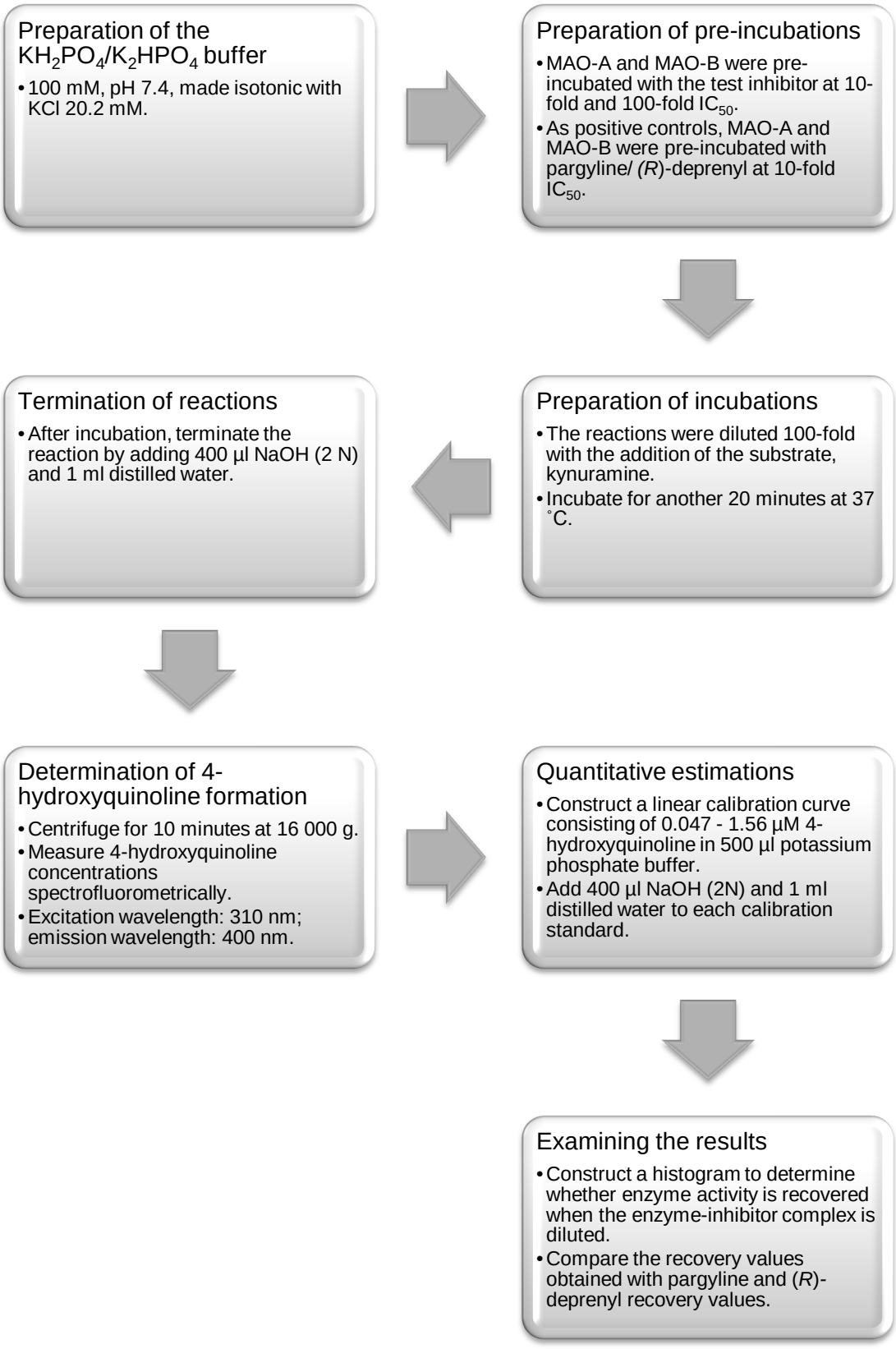

Figure 4.4.1 Diagrammatic representation of the method followed for the dilution studies.

4.5 Lineweaver-Burk plots:

Lineweaver-Burk plots can be used to determine whether an inhibitor acts competitively or noncompetitively. A set of Lineweaver-Burk plots was constructed for a selected inhibitor.

4.5.1 Method:

- Recombinant human MAO-A and MAO-B at a concentration of 5 mg/ml each, were obtained from Sigma-Aldrich, pre-aliquoted and stored at -70 ˚C. The incubations were conducted in 500 µl potassium phosphate buffer (100 mM, pH 7.4, made isotonic with KCl). DMSO (4%) was added to each reaction as co-solvent.
- Five Lineweaver-Burk plots were constructed: one plot in the absence of inhibitor and the remaining four plots in the presence of concentrations of the inhibitor equal to ¼ × IC_{50}, ½ × IC_{50}, ¾ × IC_{50} and 1¼ × IC_{50}.
- Each Lineweaver-Burk plot was constructed at eight different concentrations of kynuramine (15-250 µM).
- The reactions containing the test inhibitor and substrate were initiated with the addition of 0.015 mg/ml MAO-A or MAO-B and were incubated at 37 ˚C for 20 min.
- The reactions were terminated by the addition of 400 µl NaOH (2 N) and 1000 µl distilled water and were subsequently centrifuged at 16 000 g for 10 min.
- The initial rates by which MAO catalyzes the oxidation of kynuramine were then determined spectrofluorometrically. The concentration of 4-hydroxyquinoline in each reaction was determined by measuring the fluorescence of the supernatant at an excitation wavelength of 310 nm and an emission wavelength of 400 nm. The PMT voltage of the spectrofluorometer was set to medium with excitation and emission slit widths of 5 mm each.
- A calibration curve was constructed with 0.047-1.56 µM of 4-hydroxyquinoline dissolved in 500 µl potassium phosphate buffer (100 mM, pH 7.4, made isotonic with KCl 20.2 mM). 400 µl NaOH (2 N) and 1 ml distilled water were added to each calibration standard.
- Lineweaver-Burk plots were constructed from the data sets and a linear regression analysis was performed using the GraphPad Prism® 5 software package.

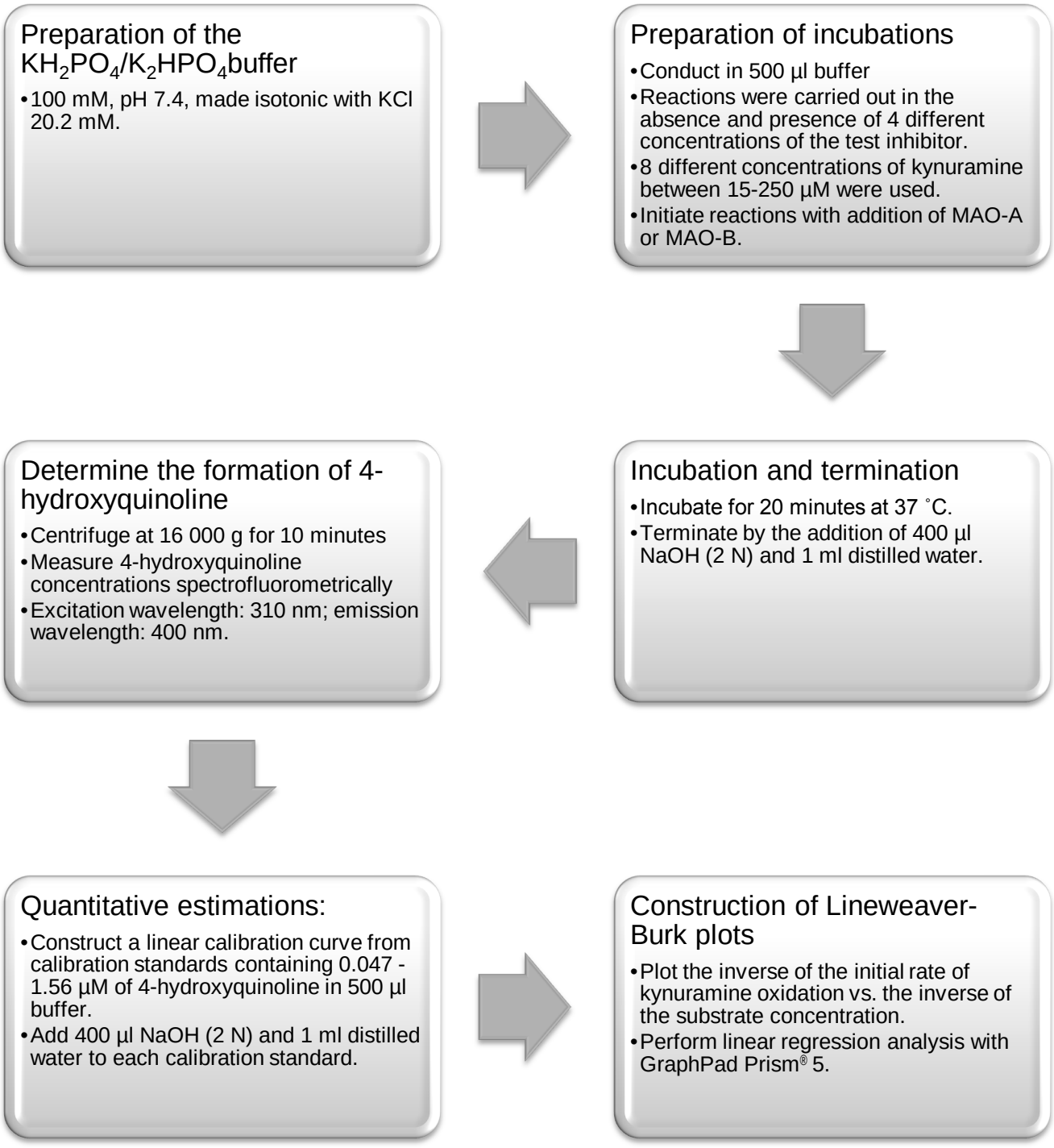

Figure 4.5.1 Diagrammatic presentation of the method used for the construction of Lineweaver-Burk plots.

4.6 Dialysis studies:

- In this study Thermo Scientific Slide-A-Lyzer dialysis cassettes with a molecular weight cut-off of 10 000 and a sample volume capacity of 0.5–3 ml were used.

- The MAO enzymes (0.03 mg/ml) and the test drug, at a concentration equal to four-fold the IC_{50} values for the inhibition of the respective enzymes, were pre-incubated for 15 min at 37 °C. These reactions were conducted in potassium phosphate buffer (100 mM, pH 7.4) containing 5% sucrose to final volumes of 0.8 ml. DMSO (4%) was added as co-solvent to all preincubations.

- As controls, MAO-A and MAO-B were similarly preincubated in the absence of inhibitor and presence of the irreversible inhibitors, pargyline and (*R*)-deprenyl, respectively. The concentrations of pargyline [IC_{50}(MAO-A) = 13 µM] (Strydom *et al.*, 2012) and (*R*)-deprenyl [IC_{50}(MAO-B) = 0.079 µM] (Petzer *et al.*, 2012) employed were equal to four-fold the IC_{50} values for the inhibition of the respective enzymes.

- The reactions (0.8 ml) were subsequently dialyzed at 4 °C in 80 ml of outer buffer (100 mM potassium phosphate, pH 7.4, 5% sucrose). The outer buffer was replaced with fresh buffer at 3 h and 7 h after the start of dialysis.

- At 24 h after dialysis was started, the reactions were diluted two-fold with the addition of kynuramine (dissolved in potassium phosphate buffer, 100 mM, pH 7.4, made isotonic with KCl). The final concentration of kynuramine in these reactions was 50 µM while the final inhibitor concentrations were equal to two-fold its IC_{50} values for the inhibition of the MAOs.

- The reactions (500 µl) were subsequently incubated for a further 20 minutes at 37 ˚C and terminated with the addition of 400 µl NaOH (2 N) and 1000 µl distilled water.

- The residual rates of 4-hydroxyquinoline formation were determined by constructing a linear calibration curve from solutions of 4-hydroxyquinoline (0.047–1.50 µM) in potassium phosphate buffer. The calibration standards were prepared to a volume of 500 µl and 400 µl NaOH (2 N) and 1000 µl distilled water were added to each standard solution.

- For comparison, undialyzed mixtures of the MAOs with the selected inhibitors were maintained at 4 °C over the same time period. All reactions were carried out in triplicate and the residual enzyme catalytic rates were expressed as mean ± SD.

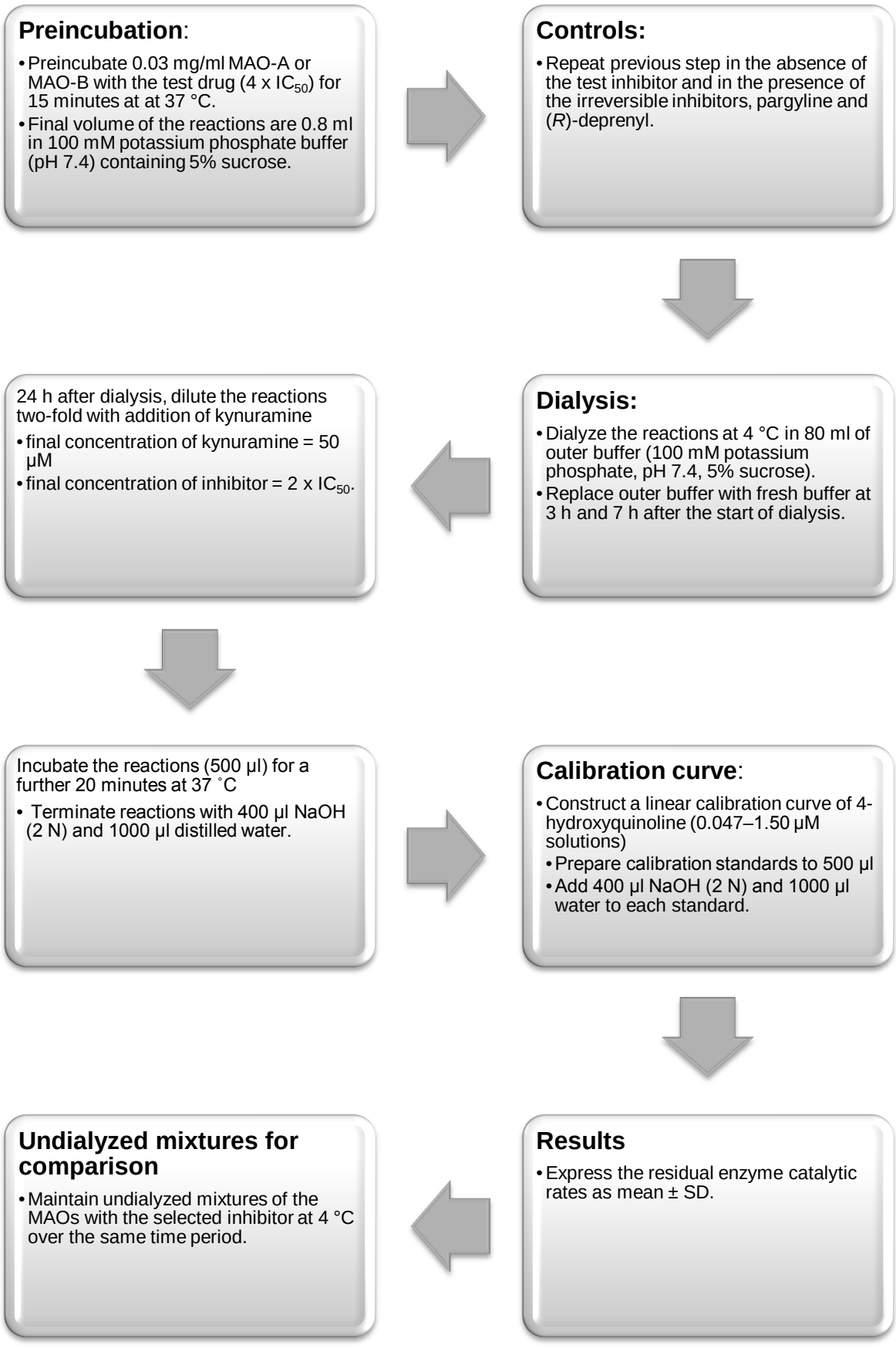

Figure 4.6.1 Diagrammatic overview of the protocol followed for the dialysis studies.

4.7 Results of the MAO inhibition studies with drugs that mapped to the *structure-based* pharmacophore models of MAO-A and MAO-B, but proved not to be inhibitors *in vitro*, or were not potent enough inhibitors to be of clinical significance:

4.7.1 2-Ethoxybenzamide:

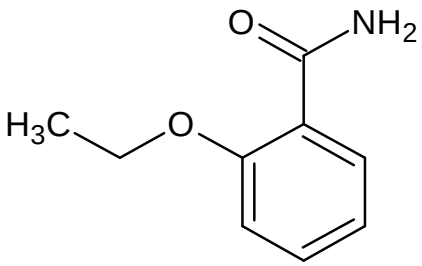

Figure 4.7.1 The structure of 2-ethoxybenzamide.

2-Ethoxybenzamide (or ethenzamide) is an analgesic and anti-inflammatory drug that is commonly used for the relief of fever, headaches and minor aches and pains. It is often used as an ingredient of cold medications. The results show that it has some inhibitory activity for MAO-A, but no activity for MAO-B even at a maximum tested concentration of 100 µM. At higher concentrations the compound itself undergoes fluorescence to the extent that an accurate IC_{50} value could not be determined.The concentration-response curves of the MAO-A and MAO-B catalytic activity in the presence of increasing concentrations of 2-ethoxybenzamide are given below.

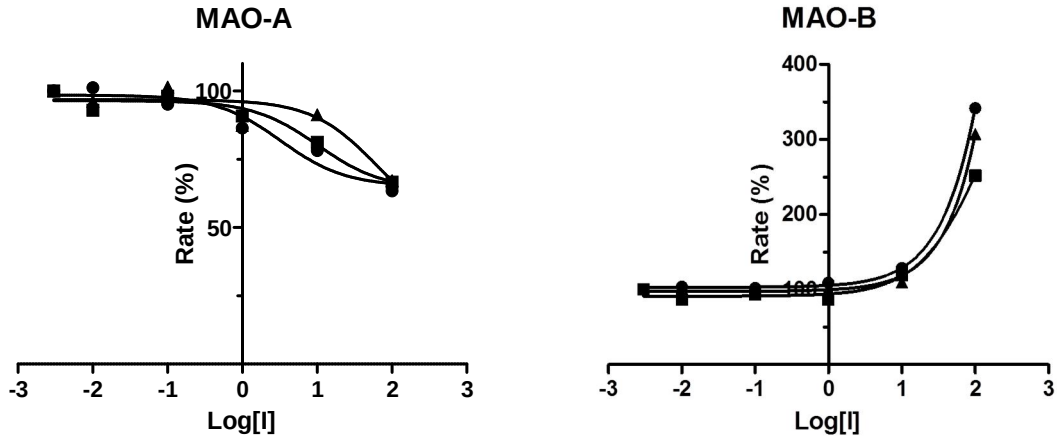

Figure 4.7.2 The recombinant human MAO-A (left) and MAO-B (right) catalyzed oxidation of kynuramine in the presence of various concentrations of 2-ethoxybenzamide (expressed in µM). The concentration-response curves were constructed in triplicate from the initial rates of kynuramine oxidation versus the logarithm of the concentration of 2-ethoxybenzamide. The rates are expressed as the percentage of the catalytic rate recorded in the absence of inhibitor.

4.7.2 Isoxsuprine:

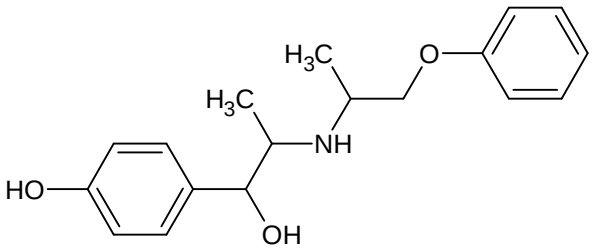

Figure 4.7.3 The structure of isoxsuprine.

Isoxsuprine is a vasodilator that is used to relieve the symptoms of central and peripheral vascular diseases like atherosclerosis. Isoxsuprine is a β-adrenergic agonist. The results show that it is not an inhibitor of either MAO-A or MAO-B even at a maximum tested concentration of 100 µM. The concentration-response curves of the MAO-A and MAO-B catalytic activity in the presence of increasing concentrations of isoxsuprine are given below.

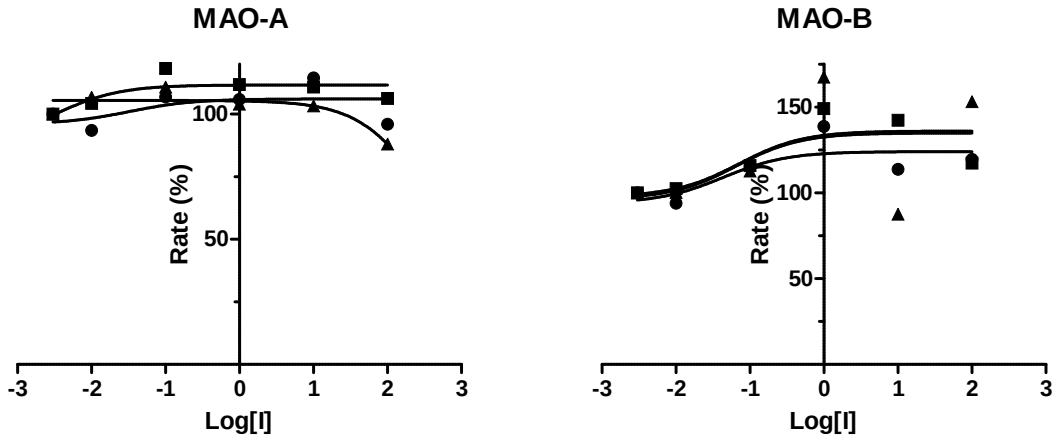

Figure 4.7.4 The recombinant human MAO-A (left) and MAO-B (right) catalyzed oxidation of kynuramine in the presence of various concentrations of isoxsuprine (expressed in µM). The concentration-response curves were constructed in triplicate from the initial rates of kynuramine oxidation versus the logarithm of the concentration of isoxsuprine. The rates are expressed as the percentage of the catalytic rate recorded in the absence of inhibitor.

4.7.3 Phenytoin:

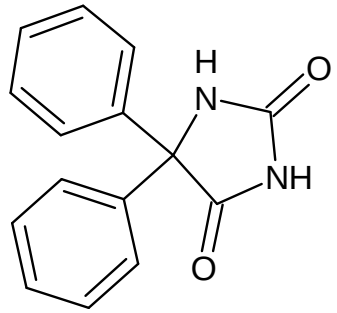

Figure 4.7.5 The structure of phenytoin.

Phenytoin is the oldest nonsedative antiseizure drug on the market. It is used for the treatment of partial seizures and generalized tonic-clonic seizures. The results show that it is not an inhibitor of MAO-B even at a maximum tested concentration of 100 µM. At higher concentrations, it showed partial inhibition of MAO-A. Its estimated IC_{50} value for the inhibition of MAO-A is 136.6 ± 55.0 µM. The concentration-response curves of the MAO-A and MAO-B catalytic activity in the presence of increasing concentrations of phenytoin are given below.

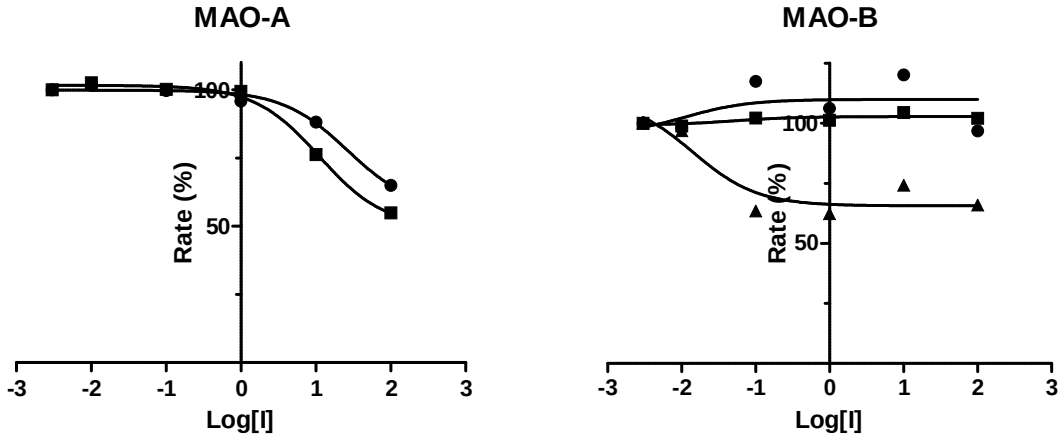

Figure 4.7.6 The recombinant human MAO-A (left) and MAO-B (right) catalyzed oxidation of kynuramine in the presence of various concentrations of phenytoin (expressed in µM). The concentration-response curves were constructed in triplicate from the initial rates of kynuramine oxidation versus the logarithm of the concentration of phenytoin. The rates are expressed as the percentage of the catalytic rate recorded in the absence of inhibitor.

4.7.4 2-benzyl-2-imidazoline:

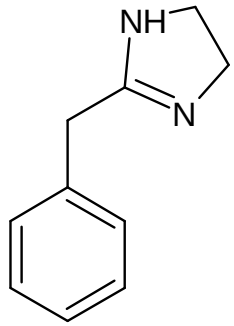

Figure 4.7.7 The structure of 2-benzyl-2-imidazoline.

2-benzyl-2-imidazoline (or tolazoline) is a vasodilator. The results show that although at very high concentrations there is a small amount of inhibitory activity towards MAO-A, it is not significant enough to estimate an IC_{50} value. The concentration-response curves of the MAO-A and MAO-B catalytic activity in the presence of increasing concentrations of 2-benzyl-2-imidazoline are given below.

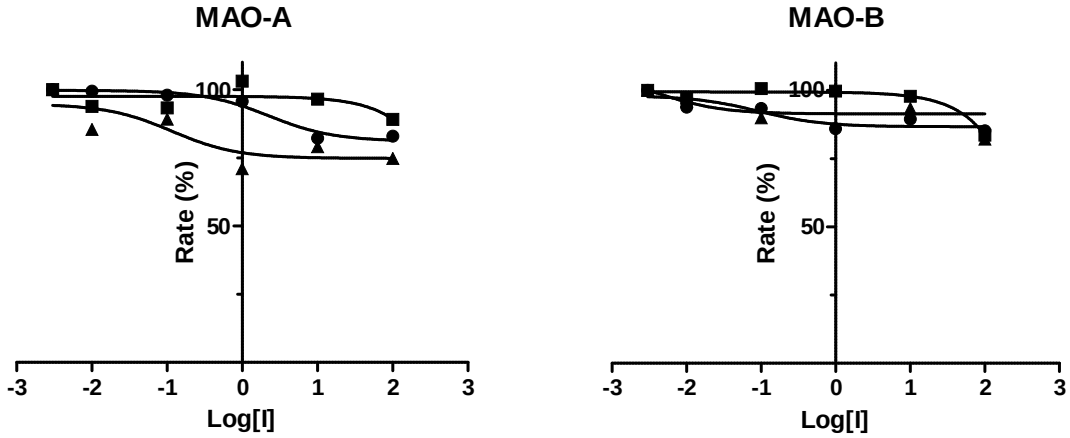

Figure 4.7.8 The recombinant human MAO-A (left) and MAO-B (right) catalyzed oxidation of kynuramine in the presence of various concentrations of 2-benzyl-2-imidazoline (expressed in μM). The concentration-response curves were constructed in triplicate from the initial rates of kynuramine oxidation versus the logarithm of the concentration of 2-benzyl-2-imidazoline. The rates are expressed as the percentage of the catalytic rate recorded in the absence of inhibitor.

4.7.5 **Mebeverine:**

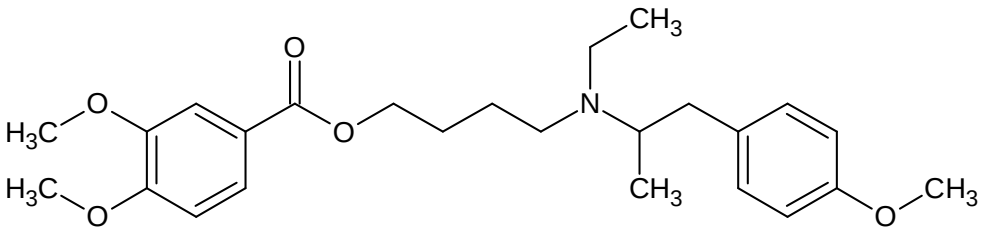

Figure 4.7.9 The structure of mebeverine.

Mebeverine is an antispasmodic drug used in the treatment of irritable bowel syndrome. The results show that at high concentrations, mebeverine has weak MAO-A and MAO-B inhibitory activities. For the inhibition of MAO-A by mebeverine an IC_{50} value of 147 ± 57.5 µM is estimated. The inhibition of MAO-B by mebeverine is not significant enough to estimate an IC_{50} value. The concentration-response curves of the MAO-A and MAO-B catalytic activity in the presence of increasing concentrations of mebeverine are given below. At high concentrations the compound itself suppressed fluorescence to a small degree.

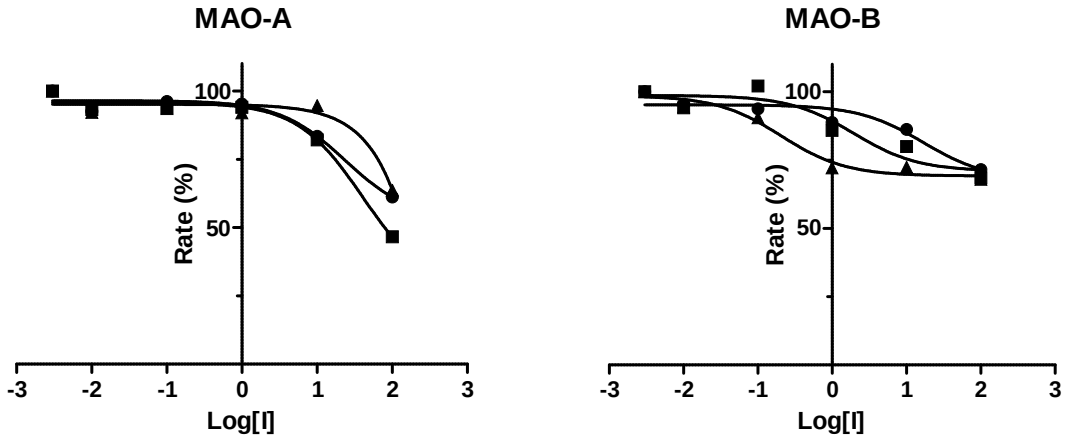

Figure 4.7.10 The recombinant human MAO-A (left) and MAO-B (right) catalyzed oxidation of kynuramine in the presence of various concentrations of mebeverine (expressed in µM). The concentration-response curves were constructed in triplicate from the initial rates of kynuramine oxidation versus the logarithm of the concentration of mebeverine. The rates are expressed as the percentage of the catalytic rate recorded in the absence of inhibitor.

4.7.6 **Amodiaquine:**

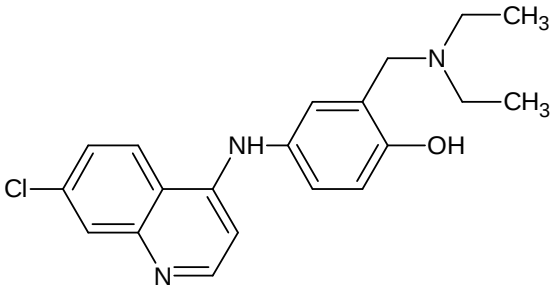

Figure 4.7.11 The structure of amodiaquine.

Amodiaquine is an antimalarial drug that is used in the treatment of chloroquine resistant *Plasmodium falciparum* malaria in combination with other drugs. The results show that amodiaquine is not a potent inhibitor of either MAO-A or MAO-B even at a maximum tested concentration of 100 µM. The inhibition of MAO-A and MAO-B by amodiaquine is not significant enough to estimate IC_{50} values. The concentration-response curves of the MAO-A and MAO-B catalytic activity in the presence of increasing concentrations of amodiaquine are given below.

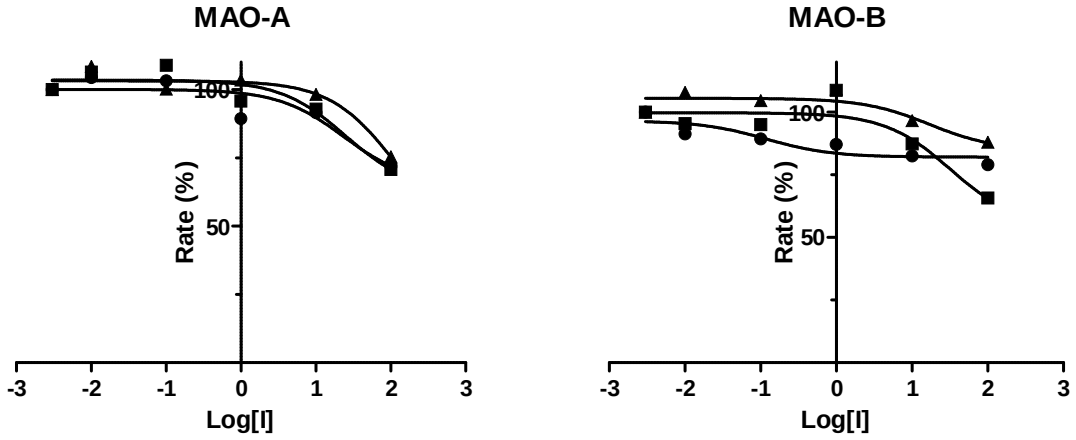

Figure 4.7.12 The recombinant human MAO-A (left) and MAO-B (right) catalyzed oxidation of kynuramine in the presence of various concentrations of amodiaquine (expressed in µM). The concentration-response curves were constructed in triplicate from the initial rates of kynuramine oxidation versus the logarithm of the concentration of amodiaquine. The rates are expressed as the percentage of the catalytic rate recorded in the absence of inhibitor.

4.7.7 **Amlodipine:**

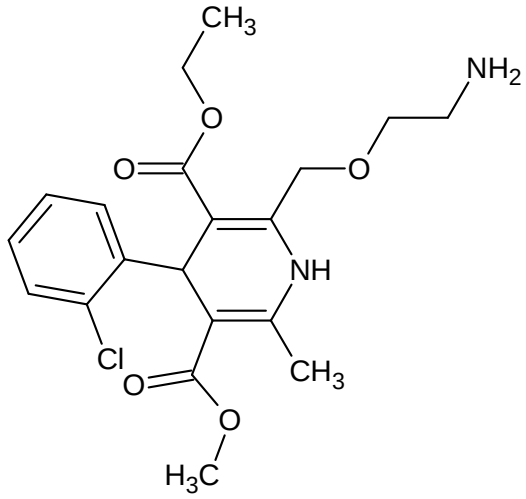

Figure 4.7.13 The structure of amlodipine.

Amlodipine is a calcium channel-blocking agent that is commonly used in cardiovascular conditions like hypertension and angina pectoris. Although the curves show good activity for MAO-A inhibition, the compound itself is a potent suppressor of fluorescence and most of the activity seen is probably as a result of the suppression of fluorescence, rather than true inhibition of MAO-A and MAO-B. The MAO inhibitory properties of amlodipine were examined at maximum concentrations of 300 µM for MAO-A and 100 µM for MAO-B.

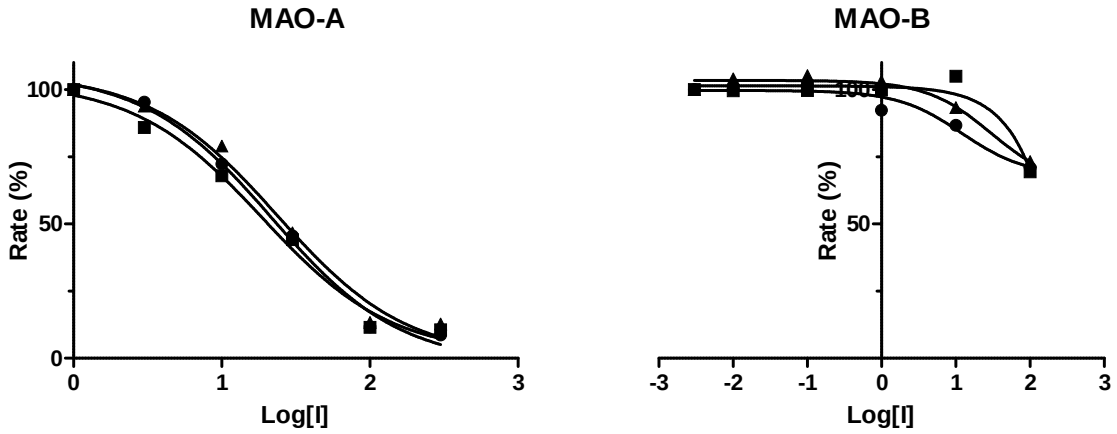

Figure 4.7.14 The recombinant human MAO-A (left) and MAO-B (right) catalyzed oxidation of kynuramine in the presence of various concentrations of amlodipine (expressed in µM). The concentration-response curves were constructed in triplicate from the initial rates of kynuramine oxidation versus the logarithm of the concentration of amlodipine. The rates are expressed as the percentage of the catalytic rate recorded in the absence of inhibitor.

4.7.8 Zafirlukast:

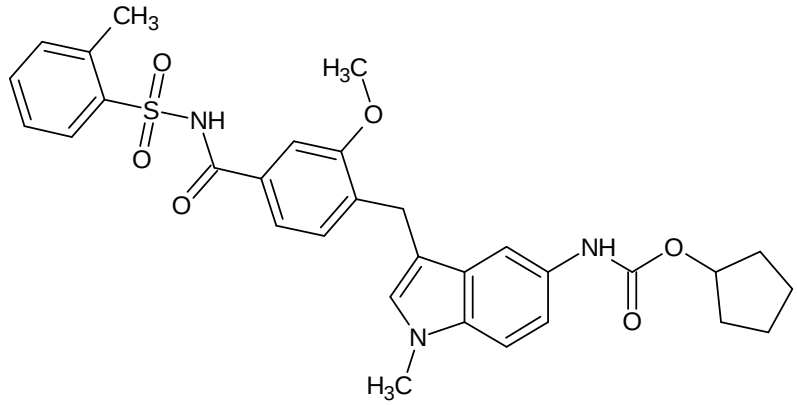

Figure 4.7.15 The structure of zafirlukast.

Zafirlukast is a leukotriene D4 receptor antagonist that is used in the treatment of asthma. The results show that, at high concentrations, zafirlukast shows some inhibitory activity towards both MAO-A and MAO-B. The IC_{50} values for the inhibition of MAO-A and MAO-B are 182 ± 13.2 µM and 144 ± 9.57 µM, respectively. The concentration-response curves of the MAO-A and MAO-B catalytic activity in the presence of increasing concentrations of zafirlukast (up to 100 µM) are given below.

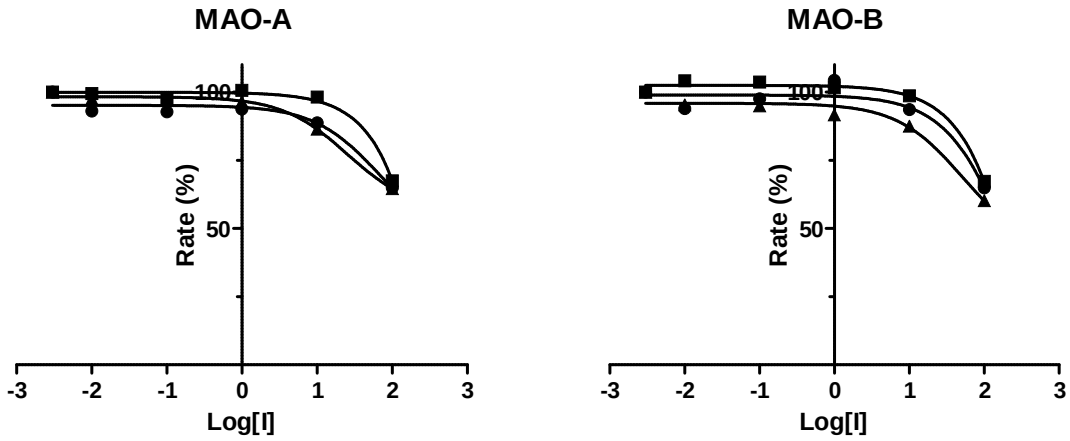

Figure 4.7.16 The recombinant human MAO-A (left) and MAO-B (right) catalyzed oxidation of kynuramine in the presence of various concentrations of zafirlukast (expressed in µM). The concentration-response curves were constructed in triplicate from the initial rates of kynuramine oxidation versus the logarithm of the concentration of zafirlukast. The rates are expressed as the percentage of the catalytic rate recorded in the absence of inhibitor.

4.7.9 Dicumarol:

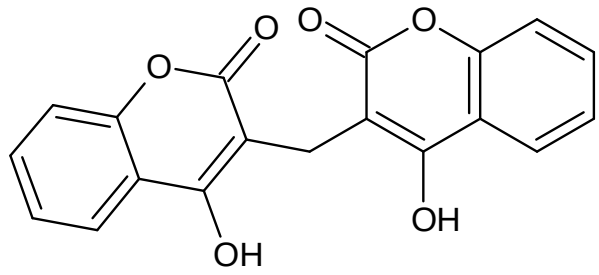

Figure 4.7.17 The structure of dicumarol.

Dicumarol is a coumarin anticoagulant sometimes used in the treatment of thrombosis. At higher doses it is used as a rodenticide. The results show that it is not an inhibitor of either MAO-A or MAO-B even at a maximum tested concentration of 100 µM. The apparent inhibitory effect seen in the graphs is due to the potent suppression of fluorescence by dicumarol itself. The concentration-response curves of the MAO-A and MAO-B catalytic activity in the presence of increasing concentrations of dicumarol are given below.

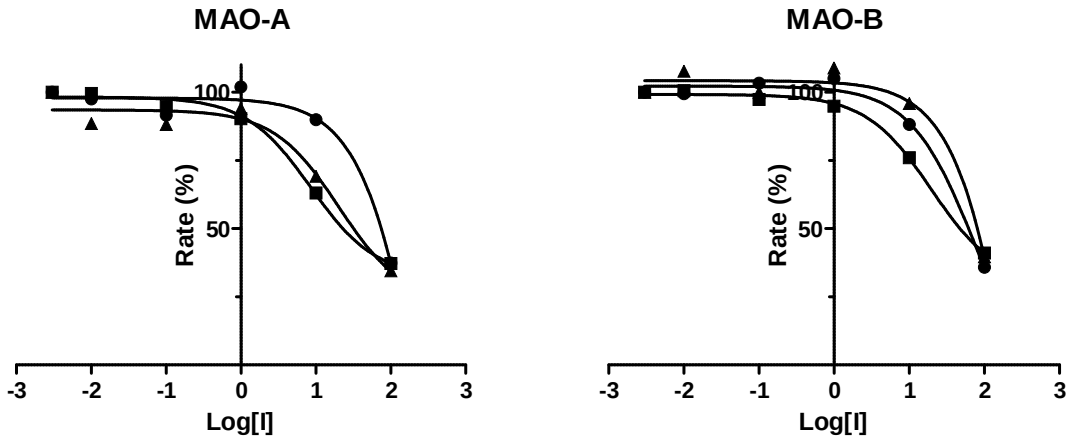

Figure 4.7.18 The recombinant human MAO-A (left) and MAO-B (right) catalyzed oxidation of kynuramine in the presence of various concentrations of dicumarol (expressed in µM). The concentration-response curves were constructed in triplicate from the initial rates of kynuramine oxidation versus the logarithm of the concentration of dicumarol. The rates are expressed as the percentage of the catalytic rate recorded in the absence of inhibitor.

4.7.10 Sulpiride:

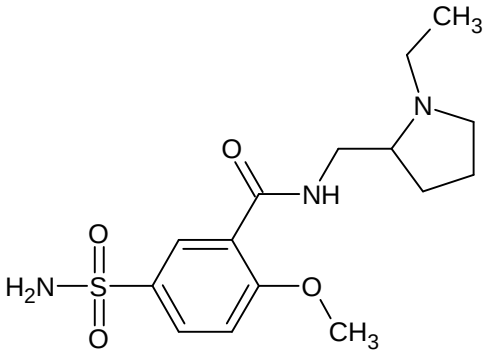

Figure 4.7.19 The structure of sulpiride.

Sulpiride is a benzamide class dopamine 2 receptor antagonist that is used in psychotic disorders such as schizophrenia. The results show that it is not an inhibitor of either MAO-A or MAO-B even at a maximum tested concentration of 100 µM. The concentration-response curves of the MAO-A and MAO-B catalytic activity in the presence of increasing concentrations of sulpiride are given below.

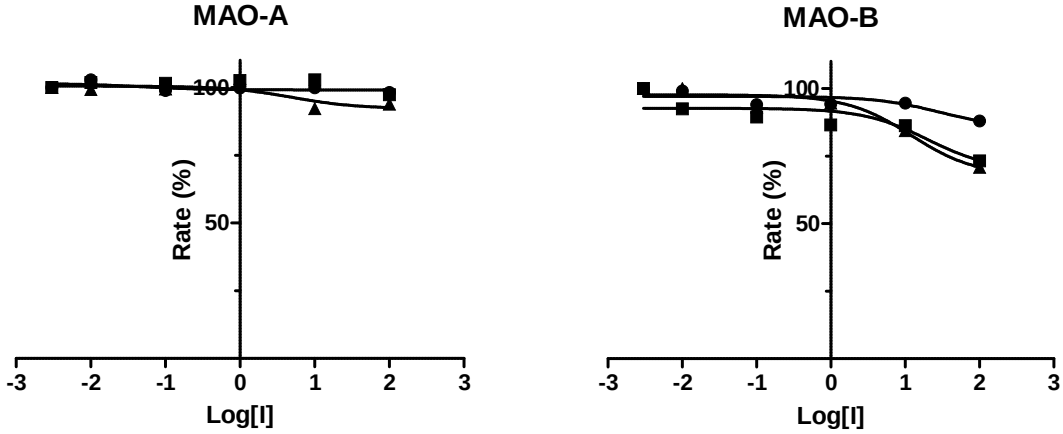

Figure 4.7.20 The recombinant human MAO-A (left) and MAO-B (right) catalyzed oxidation of kynuramine in the presence of various concentrations of sulpiride (expressed in µM). The concentration-response curves were constructed in triplicate from the initial rates of kynuramine oxidation versus the logarithm of the concentration of sulpiride. The rates are expressed as the percentage of the catalytic rate recorded in the absence of inhibitor.

4.7.11 Cefotaxime:

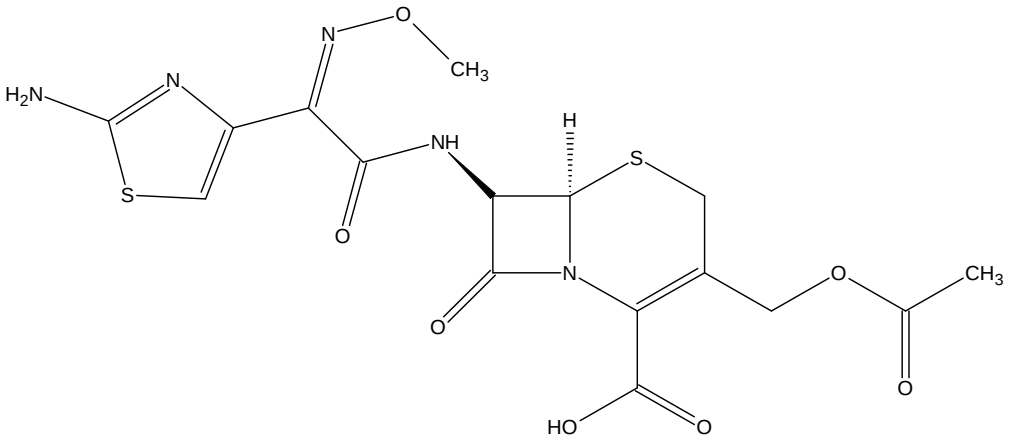

Figure 4.7.21 The structure of cefotaxime.

Cefotaxime is a third generation cephalosporin antibiotic used for the treatment of Gram-positive and Gram-negative infections. The results show that it is not an inhibitor of either MAO-A or MAO-B even at a maximum tested concentration of 100 µM. The concentration-response curves of the MAO-A and MAO-B catalytic activity in the presence of increasing concentrations of cefotaxime are given below.

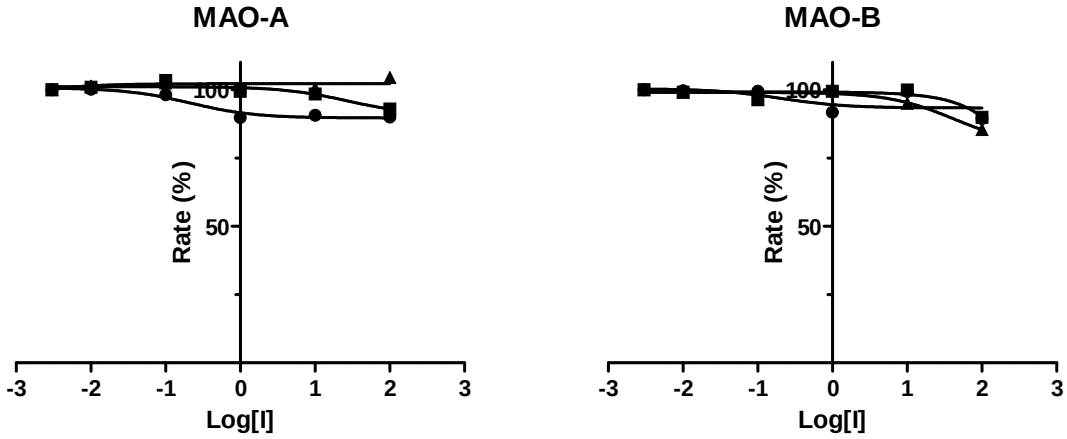

Figure 4.7.22 The recombinant human MAO-A (left) and MAO-B (right) catalyzed oxidation of kynuramine in the presence of various concentrations of cefotaxime (expressed in µM). The concentration-response curves were constructed in triplicate from the initial rates of kynuramine oxidation versus the logarithm of the concentration of cefotaxime. The rates are expressed as the percentage of the catalytic rate recorded in the absence of inhibitor.

4.7.12 Cefuroxime:

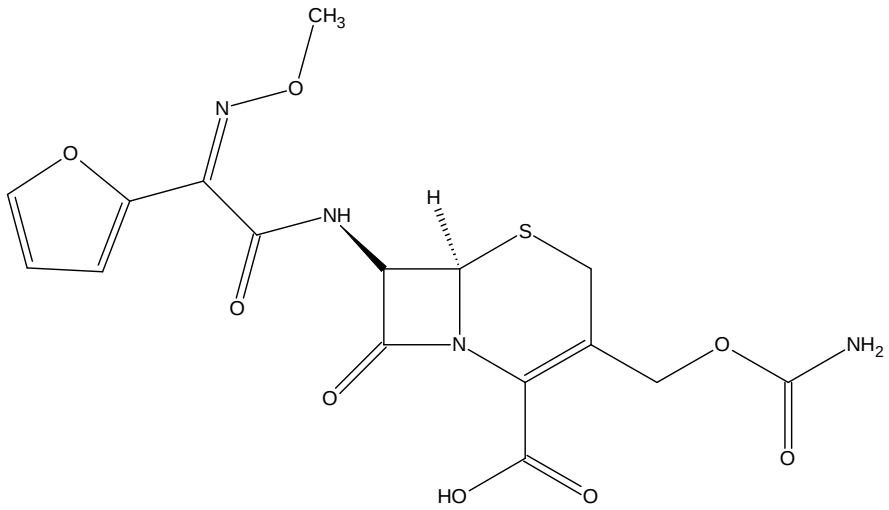

Figure 4.7.23 The structure of cefuroxime.

Cefuroxime is a second generation cephalosporin antibiotic. The results show that it is not an inhibitor of either MAO-A or MAO-B even at a maximum tested concentration of 100 µM. The concentration-response curves of the MAO-A and MAO-B catalytic activity in the presence of increasing concentrations of cefuroxime are given below.

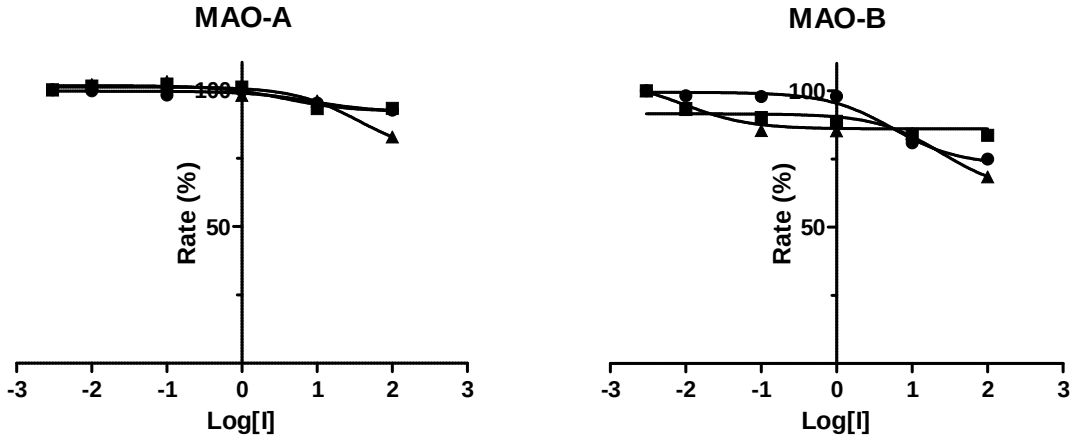

Figure 4.7.24 The recombinant human MAO-A (left) and MAO-B (right) catalyzed oxidation of kynuramine in the presence of various concentrations of cefuroxime (expressed in µM). The concentration-response curves were constructed in triplicate from the initial rates of kynuramine oxidation versus the logarithm of the concentration of cefuroxime. The rates are expressed as the percentage of the catalytic rate recorded in the absence of inhibitor.

4.7.13 **Sumatriptan**:

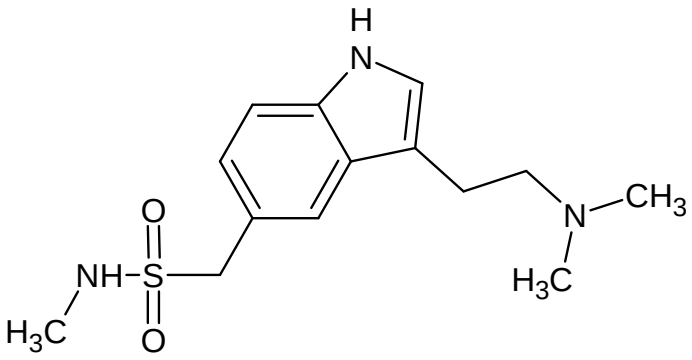

Figure 4.7.25 The structure of sumatriptan.

Sumatriptan is a selective serotonin 1 receptor agonist that is used in the treatment of acute migraines. The results show that it is not a significant inhibitor of either MAO-A or MAO-B even at a maximum tested concentration of 100 µM. Although a small degree of MAO-A inhibition was observed with one of the replicate curves, this is not significant enough to estimate an IC_{50} value. The concentration-response curves of the MAO-A and MAO-B catalytic activity in the presence of increasing concentrations of sumatriptan are given below.

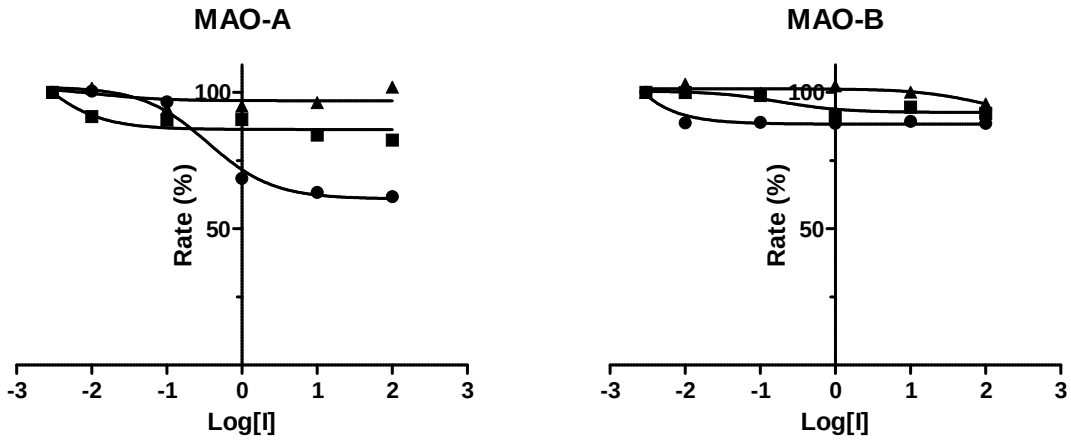

Figure 4.7.26 The recombinant human MAO-A (left) and MAO-B (right) catalyzed oxidation of kynuramine in the presence of various concentrations of sumatriptan (expressed in µM). The concentration-response curves were constructed in triplicate from the initial rates of kynuramine oxidation versus the logarithm of the concentration of sumatriptan. The rates are expressed as the percentage of the catalytic rate recorded in the absence of inhibitor.

4.7.14 Valpromide:

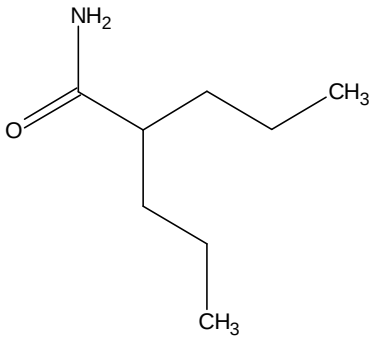

Figure 4.7.27 The structure of valpromide.

Valpromide is a derivative of the better known valproic acid. The uses of valpromide includes the treatment of epilepsy, the prophylaxis of migraines and the treatment of the manic phase of bipolar disorder. The results show that it is not an inhibitor of either MAO-A or MAO-B even at a maximum tested concentration of 100 µM. The concentration-response curves of the MAO-A and MAO-B catalytic activity in the presence of increasing concentrations of valpromide are given below.

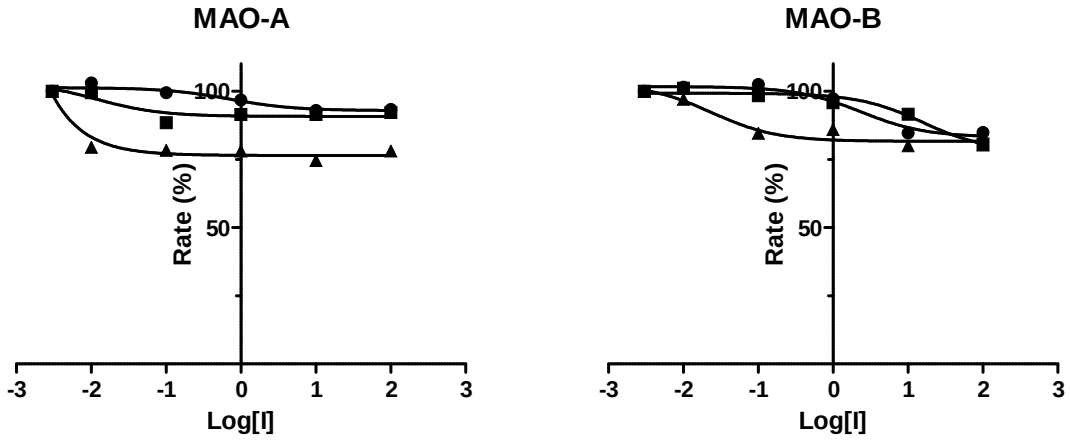

Figure 4.7.28 The recombinant human MAO-A (left) and MAO-B (right) catalyzed oxidation of kynuramine in the presence of various concentrations of valpromide (expressed in µM). The concentration-response curves were constructed in triplicate from the initial rates of kynuramine oxidation versus the logarithm of the concentration valpromide. The rates are expressed as the percentage of the catalytic rate recorded in the absence of inhibitor.

4.7.15 **Papaverine**:

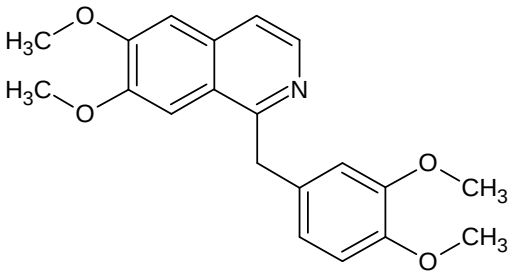

Figure 4.7.29 The structure of papaverine.

Papaverine is an opium alkaloid antispasmodic drug that is used in the treatment of visceral spasms, vasospasms and erectile dysfunction. The results show that at high concentrations it displays some inhibition of MAO-A (with an IC_{50} value of 99.2 ± 8.67 µM), but no inhibition of MAO-B. It was tested at a maximal concentration of 100 µM. Complete suppression of MAO-A activity could not be achieved at this concentration. The concentration-response curves of the MAO-A and MAO-B catalytic activity in the presence of increasing concentrations of papaverine are given below.

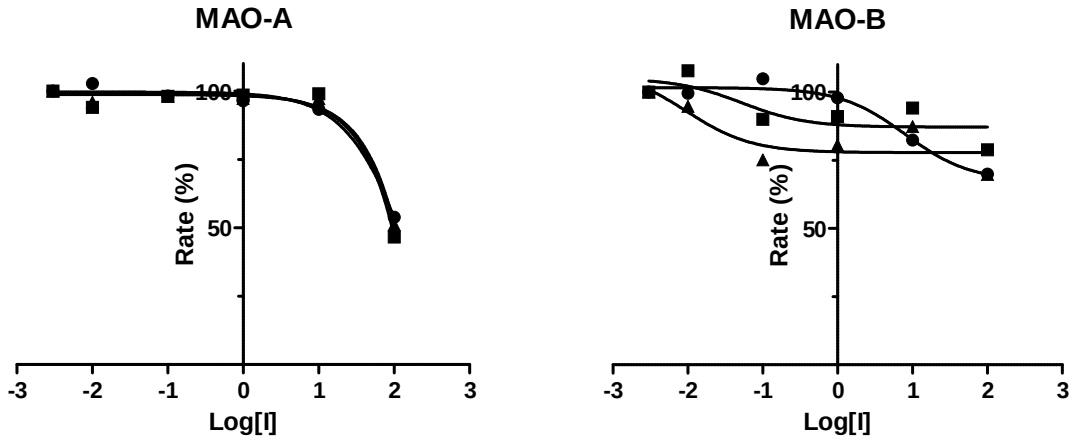

Figure 4.7.30 The recombinant human MAO-A (left) and MAO-B (right) catalyzed oxidation of kynuramine in the presence of various concentrations of papaverine (expressed in µM). The concentration-response curves were constructed in triplicate from the initial rates of kynuramine oxidation versus the logarithm of the concentration of papaverine. The rates are expressed as the percentage of the catalytic rate recorded in the absence of inhibitor.

4.7.16 Ranolazine:

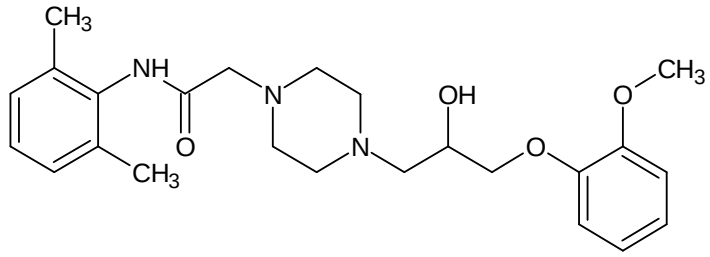

Figure 4.7.31 The structure of ranolazine.

Ranolazine is used in the treatment of chronic angina pectoris. The results show that it is not an inhibitor of either MAO-A or MAO-B even at a maximum tested concentration of 100 µM. The concentration-response curves of the MAO-A and MAO-B catalytic activity in the presence of increasing concentrations of ranolazine are given below.

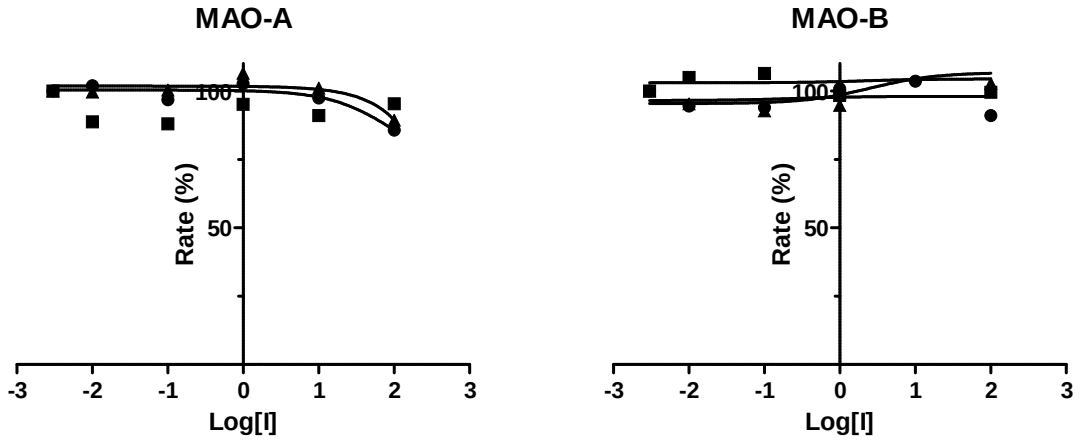

Figure 4.7.32 The recombinant human MAO-A (left) and MAO-B (right) catalyzed oxidation of kynuramine in the presence of various concentrations of ranolazine (expressed in µM). The concentration-response curves were constructed in triplicate from the initial rates of kynuramine oxidation versus the logarithm of the concentration of ranolazine. The rates are expressed as the percentage of the catalytic rate recorded in the absence of inhibitor.

4.7.17 Clofibrate:

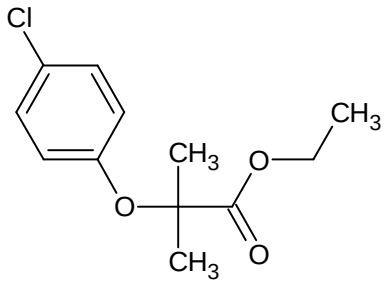

Figure 4.7.33 The structure of clofibrate.

Clofibrate is a lipid-lowering agent used for the treatment of high cholesterol and triglyceride levels. The results show that it acts as a weak inhibitor of both MAO-A and MAO-B at a maximal tested concentration of 100 µM but complete inhibition was not achieved. The IC_{50} values estimated for the inhibition of MAO-A and MAO-B are 827 ± 856 µM and 265 ± 41.0 µM, respectively. The large deviation observed for the IC_{50} value for MAO-A inhibition is due to the observation that only one replicate curve showed slight inhibition. According to the other two replicate curves, clofibrate does not act as a MAO-A inhibitor. The concentration-response curves of the MAO-A and MAO-B catalytic activity in the presence of increasing concentrations of clofibrate are given below.

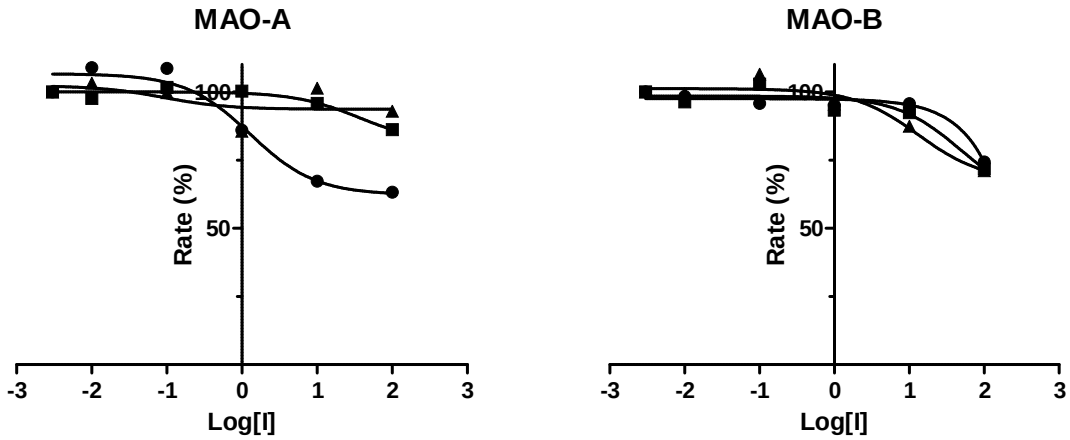

Figure 4.7.34 The recombinant human MAO-A (left) and MAO-B (right) catalyzed oxidation of kynuramine in the presence of various concentrations of clofibrate (expressed in µM). The concentration-response curves were constructed in triplicate from the initial rates of kynuramine oxidation versus the logarithm of the concentration of clofibrate. The rates are expressed as the percentage of the catalytic rate recorded in the absence of inhibitor.

4.7.18 Fursultiamine:

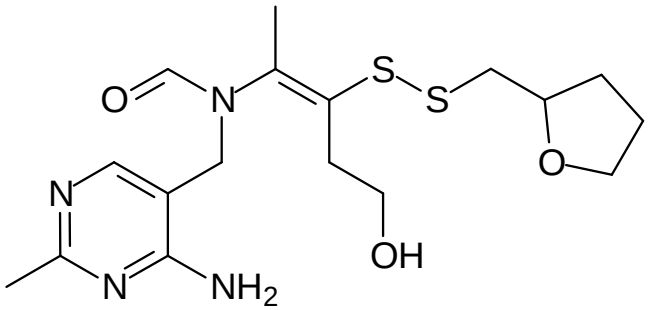

Figure 4.7.35 The structure of fursultiamine.

Fursultiamine is a disulfide derivative of tiamine (vitamin B_1). It is used in the treatment of vitamin B_1 deficiency. The results show that it is not an inhibitor of either MAO-A or MAO-B even at a maximum tested concentration of 100 µM. The concentration-response curves of

the MAO-A and MAO-B catalytic activity in the presence of increasing concentrations of fursultiamine are given below.

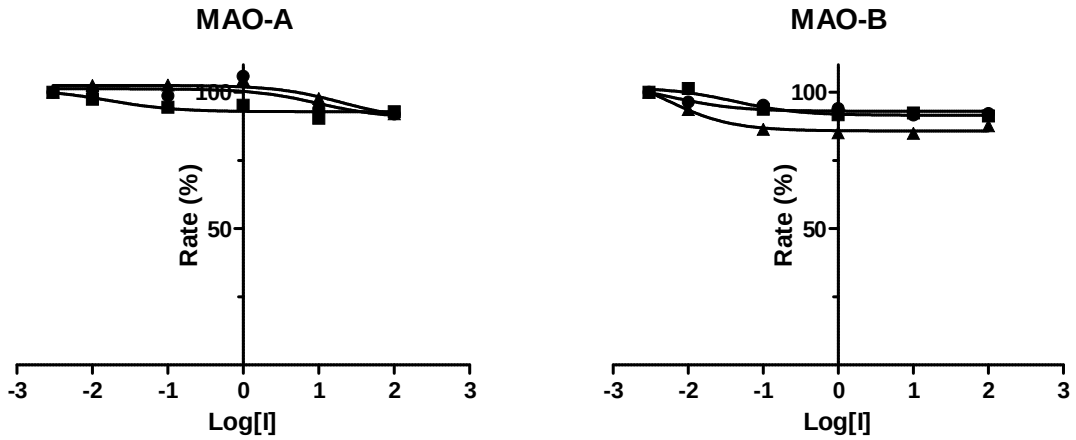

Figure 4.7.36 The recombinant human MAO-A (left) and MAO-B (right) catalyzed oxidation of kynuramine in the presence of various concentrations of fursultiamine (expressed in µM). The concentration-response curves were constructed in triplicate from the initial rates of kynuramine oxidation versus the logarithm of the concentration of fursultiamine. The rates are expressed as the percentage of the catalytic rate recorded in the absence of inhibitor.

4.7.19 Griseofulvin:

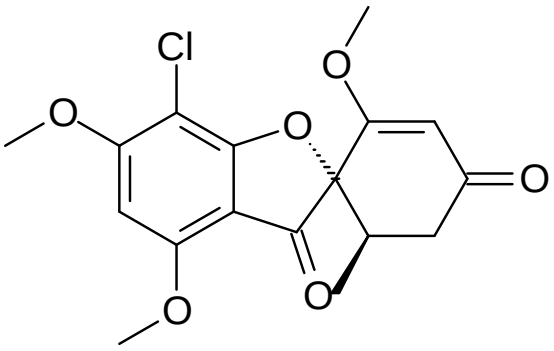

Figure 4.7.37 The structure of griseofulvin.

Griseofulvin is an antifungal antibiotic used in the treatment of common dermatophytes. The results show that it is a weak inhibitor of both MAO-A and MAO-B, but complete suppression of activity could not be achieved at the maximum tested concentration of 100 µM. The IC_{50} values estimated for the inhibition of MAO-A and MAO-B are 325 ± 36.0 µM and 356 ± 167 µM, respectively. The concentration-response curves of the MAO-A and MAO-B catalytic activity in the presence of increasing concentrations of griseofulvin are given below.

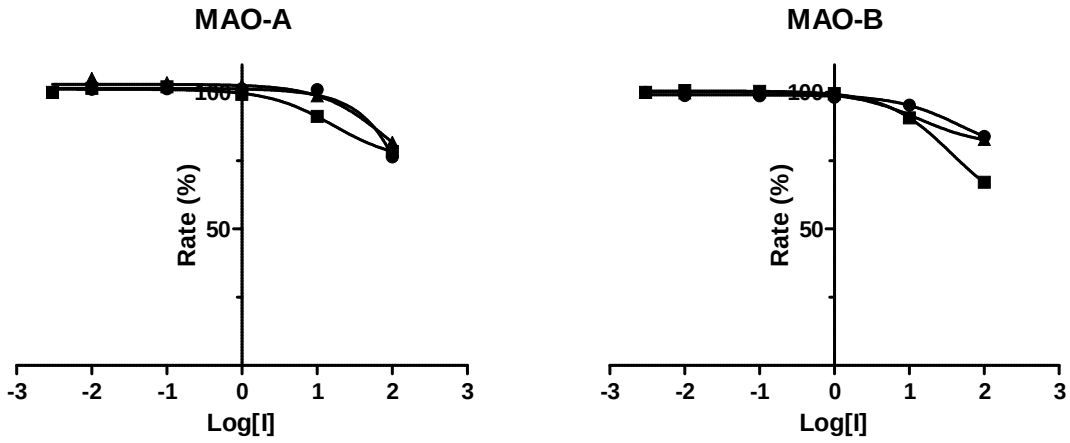

Figure 4.7.38 The recombinant human MAO-A (left) and MAO-B (right) catalyzed oxidation of kynuramine in the presence of various concentrations of griseofulvin (expressed in µM). The concentration-response curves were constructed in triplicate from the initial rates of kynuramine oxidation versus the logarithm of the concentration of griseofulvin. The rates are expressed as the percentage of the catalytic rate recorded in the absence of inhibitor.

4.7.20 Bisoprolol:

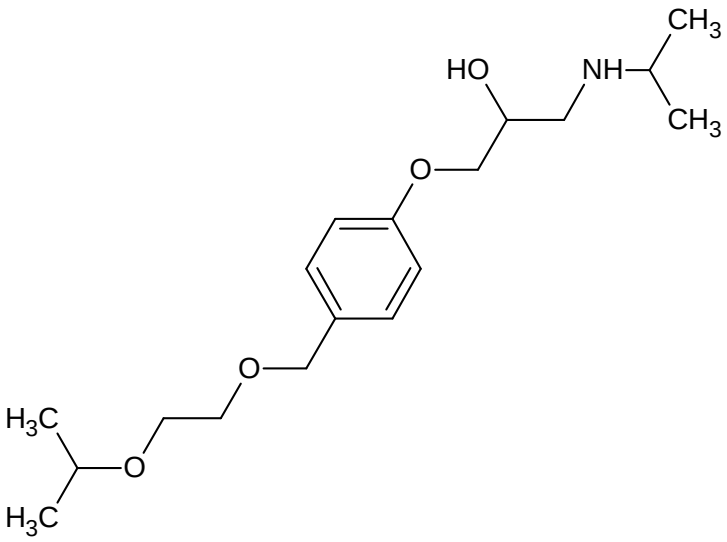

Figure 4.7.39 The structure of bisoprolol.

Bisoprolol is a β_1-adrenergic receptor antagonist used in the treatment of cardiovascular diseases such as hypertension, angina pectoris and arrhythmias. The results show that it is not a significant inhibitor of either MAO-A or MAO-B even at a maximum tested concentration of 100 µM. The concentration-response curves of the MAO-A and MAO-B catalytic activity in the presence of increasing concentrations of bisoprolol are given below.

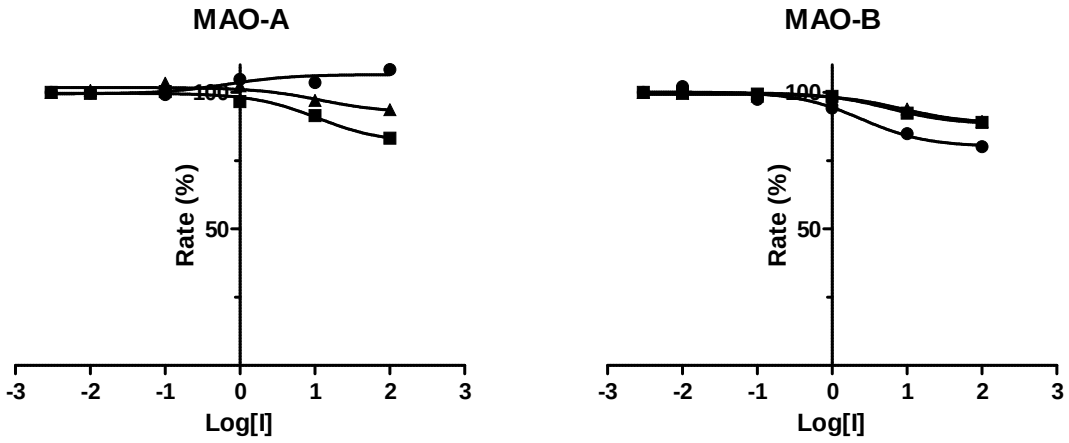

Figure 4.7.40 The recombinant human MAO-A (left) and MAO-B (right) catalyzed oxidation of kynuramine in the presence of various concentrations of bisoprolol (expressed in μM). The concentration-response curves were constructed in triplicate from the initial rates of kynuramine oxidation versus the logarithm of the concentration of bisoprolol. The rates are expressed as the percentage of the catalytic rate recorded in the absence of inhibitor.

Results of the MAO inhibition studies with drugs that mapped to the *structure-based* pharmacophore model of MAO-A and MAO-B and proved to be inhibitors *in vitro*:

4.7.21 Pentamidine:

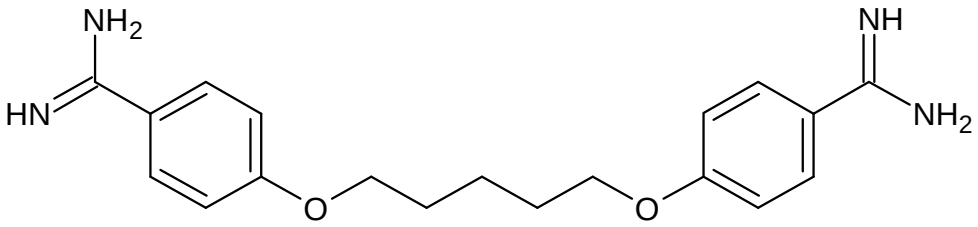

Figure 4.7.41 The structure of pentamidine.

Pentamidine is an antibiotic used in the treatment of pneumocystis pneumonia and West African trypanosomiasis. Blaschko & Duthie (1945) first reported that pentamidine inhibited rabbit liver amine oxidase. Davison (1958) used rat liver mitochondrial MAO and found that the mode of inhibition of pentamidine was non-competitive and irreversible. She also found that an injection of pentamidine strongly inhibited rat liver MAO activity, but there was only slight inhibition of brain MAO activity. However, inhibition studies with the human form of the MAO enzymes have not been done for pentamidine yet.

The results show that pentamidine, as the isethionate salt, is a potent inhibitor of both human MAO-A and MAO-B with inhibitory activities well below the maximum tested concentration of 100 µM. The IC_{50} values for the inhibition of MAO-A and MAO-B are 0.607 ± 0.010 µM and 0.220 ± 0.046 µM, respectively. The concentration-response curves of the MAO-A and MAO-B catalytic activities in the presence of increasing concentrations of pentamidine are given below. The graph shows that there is a decrease in the catalytic activities of both MAO-A and MAO-B with increasing concentrations of pentamidine. Based on its relatively good MAO inhibition potencies, the interactions of pentamidine with these enzymes were thus further investigated. Particular emphasis was placed on the reversibility of MAO inhibition by pentamidine. As mentioned above, pentamidine is reported to act as an irreversible inhibitor of rat MAO. The interactions of pentamidine with the MAOs will be further discussed in Chapter 5 where these results will be presented in article format.

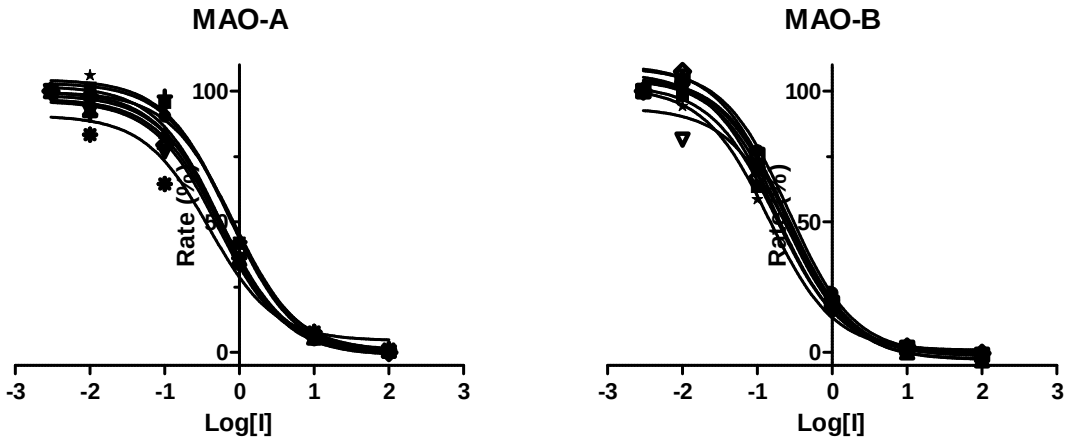

Figure 4.7.42 The recombinant human MAO-A (left) and MAO-B (right) catalyzed oxidation of kynuramine in the presence of various concentrations of pentamidine (expressed in µM). Nine concentration-response curves were constructed from the initial rates of kynuramine oxidation versus the logarithm of the concentration of the pentamidine. The rates are expressed as the percentage of the catalytic rate recorded in the absence of inhibitor.

The reversibility of the interactions of pentamidine with MAO-A and MAO-B were further investigated by evaluating the recovery of the enzymatic activity after dilution of the enzyme-inhibitor complexes. For this purpose, MAO-A and MAO-B were preincubated with pentamidine at concentrations of 10 × IC_{50} and 100 × IC_{50} for 30 min. The reactions were subsequently diluted 100-fold to 0.1 × IC_{50} and 1 × IC_{50}, respectively. The results are given in figure 4.7.43 and are indicative of the reversible inhibition of MAO-A and MAO-B because enzyme activity was recovered after dilution of the inhibitor. After dilution of pentamidine to 0.1 × IC_{50} and 1 × IC_{50}, the MAO-A catalytic activities are recovered to 95% and 62%, respectively, of the control value. For comparison, after similar treatment of MAO-A with the irreversible inhibitor pargyline (at 10 × IC_{50}) and dilution of the resulting complexes to 0.1 × IC_{50}, MAO-A activity is not recovered (1% of control). After dilution of pentamidine to 0.1 × IC_{50} and 1 × IC_{50}, the MAO-B catalytic activities are recovered to 81% and 52%, respectively, of the control value. For comparison, after similar treatment of MAO-B with the irreversible inhibitor (*R*)-deprenyl (at 10 × IC_{50}) and dilution of the resulting complexes to 0.1 × IC_{50}, MAO-B activity is not recovered (8% of control). It may thus be concluded that pentamidine interacts reversibly with both MAO-A and MAO-B. For reversible enzyme inhibition, the enzyme activities are expected to recover to levels of approximately 90% and 50%, respectively, after dilution of the inhibitor to 0.1 × IC_{50} and 1 × IC_{50}.

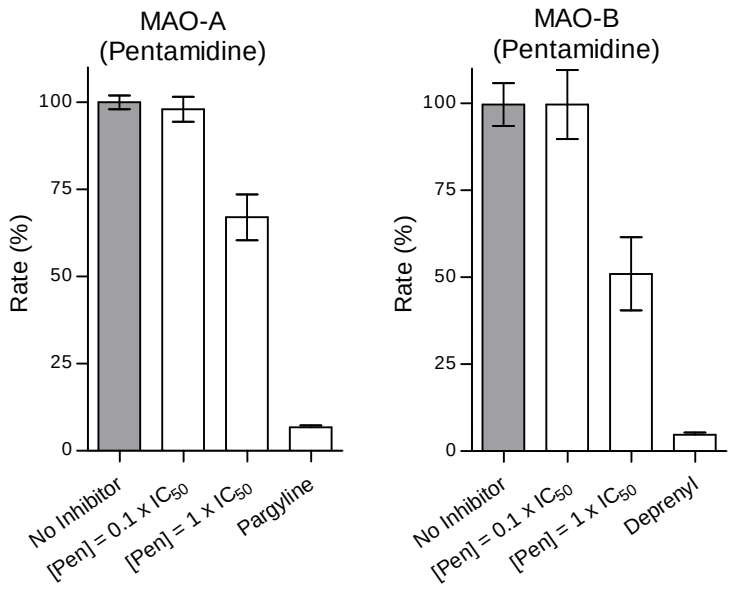

Figure 4.7.43 Reversibility of inhibition of MAO-A and MAO-B by pentamidine. The enzyme was preincubated with the test inhibitor at 10 × IC_{50} and 100 × IC_{50} for 30 min and then diluted to 0.1 × IC_{50} and 1 × IC_{50}, respectively. As controls, MAO-A and MAO-B were also preincubated with pargyline and (*R*)-deprenyl, respectively, at 10 × IC_{50} and subsequently diluted to 0.1 × IC_{50}. The residual enzyme activities were subsequently measured.

The reversibility of MAO-A and MAO-B inhibition by pentamidine was also investigated by measuring the recoveries of enzyme activities after dialysis of enzyme-inhibitor mixtures (Harfenist *et al*., 1996). The MAO enzymes and pentamidine, at a concentration of 4 × IC_{50}, were preincubated for a period of 15 min and subsequently dialyzed for 24 h. The results, given in Fig. 4.7.44, show that MAO-A and MAO-B inhibition by pentamidine is almost completely reversed after 24 h of dialysis with the MAO-A and MAO-B activities recovering to levels of 106.7% and 125% of the control values, respectively. In contrast, the MAO-A and MAO-B activities in undialyzed mixtures of the enzymes with pentamidine are both recovered to 28.7% of the control values. This behaviour is consistent with a reversible interaction between the MAO enzymes and pentamidine. For comparison, after similar preincubation and dialysis of MAO-A and MAO-B with the irreversible inhibitors, pargyline and (*R*)-deprenyl, respectively, the enzyme activities are not recovered. After dialysis of MAO-A–pargyline and MAO-B–(*R*)-deprenyl mixtures, the residual enzyme activities are only 1.5% and 2.2%, respectively, of the control values.

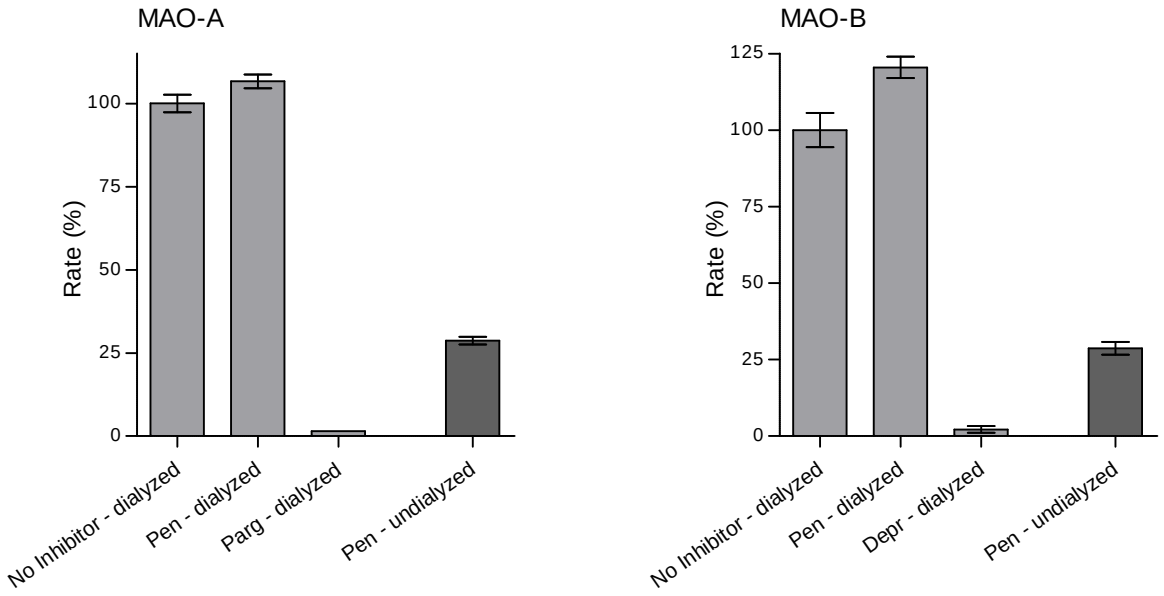

Figure 4.7.44 Reversibility of inhibition of MAO-A and MAO-B by pentamidine. The MAO enzymes and pentamidine, at an inhibitor concentration of 4 × IC_{50}, were preincubated together, dialyzed and the residual MAO activities were subsequently measured (Pen–dialyzed). For comparison, the MAO-A and MAO-B were similarly preincubated in the absence (No inhibitor–dialyzed) and presence of the irreversible inhibitors, pargyline (Parg–dialyzed) and (*R*)-deprenyl (Depr–dialyzed), respectively, and dialyzed. The residual MAO activities of undialyzed mixtures (Pen–undialyzed) of the MAOs with pentamidine are also shown.

Sets consisting of five Lineweaver–Burk plots (1/V vs. 1/[S]) were constructed to evaluate the modes of MAO inhibition of pentamidine. This kinetic analysis was also used to measure K_i values for the binding of pentamidine to the MAO enzymes. For each set of Lineweaver–Burk plots, the first plot was constructed in the absence of inhibitor, while the remaining four plots were constructed in the presence of different concentrations of pentamidine. The concentrations of the test inhibitors were ¼ × IC_{50}, ½ × IC_{50}, ¾ × IC_{50} and 1¼ × IC_{50} for the inhibition of the MAO enzymes. Kynuramine at eight different concentrations (15–250 μM) served as substrate and the concentrations of recombinant human MAO-A and MAO-B employed were 0.015 mg/ml. The rates of formation of the MAO-generated 4-hydroxyquinoline were measured by fluorescence spectrophotometry as described above. Linear regression analysis was performed using Prism 5® (Manley-King *et al*., 2011). K_i values were estimated from the x-axis intercept ($-K_i$) of a replot of the slopes of the Lineweaver–Burk plots versus inhibitor concentration. Figure 4.7.45 illustrates the sets of Lineweaver–Burk plots that were obtained from these studies. The results show that, for the inhibition of both MAO-A and MAO-B, the Lineweaver–Burk plots are linear and intersect at a single point on the y-axis. This suggests that pentamidine most likely interacts

competitively with both MAO isozymes. From the replot of the slopes of the Lineweaver–Burk plots versus the inhibitor concentrations, K_i values of 0.41 µM and 0.224 µM are estimated for the inhibition of MAO-A and MAO-B, respectively, by pentamidine.

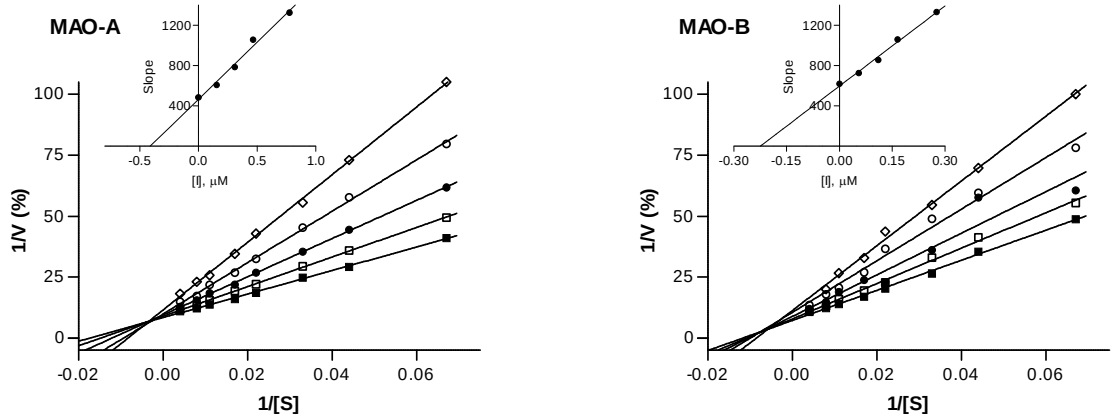

Figure 4.7.45 Lineweaver-Burk plots of human MAO-A and MAO-B activities in the absence (filled squares) and presence of various concentrations of pentamidine. For these studies the concentrations of pentamidine employed were ¼ × IC_{50}, ½ × IC_{50}, ¾ × IC_{50} and 1¼ × IC_{50}. The insets are the graphs of the slopes of the Lineweaver-Burk plots versus inhibitor concentration.

To provide additional insight, the binding modes of pentamidine within the active site cavities of MAO-A and MAO-B were examined. The molecular docking simulations were carried out according the protocol given in Chapter 3. The results are given in figures 4.7.46 and 4.7.47 and table 4.7.1 and table 4.7.2. In the active site of MAO-A, there is a hydrogen bond interaction between one of the phenolic oxygens of pentamidine and the amidic hydrogen of Val-210. There are hydrophobic interactions between pentamidine and Tyr-69 (-1.119 kcal/mol), Val-93 (-2.830 kcal/mol), Gly-110 (-3.142 kcal/mol), Ala-111 (-2.679 kcal/mol), Ile-180 (-2.562 kcal/mol), Phe-208 (-5.171 kcal/mol), Ser-209 (-3.143 kcal/mol), Val-210 (-3.327 kcal/mol), Thr-211 (-3.199 kcal/mol), Gln-215 (-3.854 kcal/mol), Ile-335 (-2.763 kcal/mol) and Phe-352 (-1.970 kcal/mol). These interactions may be observed as the cyan shaded spheres in the two dimensional representation and the negative interaction energies in the table. The interactions with Ile-180, Phe-208, Thr-211 and Gln-215 are particularly important, as seen from the more negative binding energies. There are no pi-pi interactions between pentamidine and the active site residues of MAO-A.

In the active site of MAO-B, pentamidine undergoes a hydrogen bond donor interaction with Glu-84 (-3.094 kcal/mol) and both a hydrogen bond donor and a hydrogen bond acceptor interaction with Thr-201 (-0.095 kcal/mol) as can be seen from the two dimensional diagram. There are significant hydrophobic interactions between pentamidine and Leu-171 (-4.212 kcal/mol), Ile-199 (-3.205 kcal/mol), Gln-206 (-3.114 kcal/mol), Tyr-326 (-1.781 kcal/mol) and

Tyr-398 (-1.508 kcal/mol) as seen from the cyan spheres around the residues in the two dimensional diagram. Other significant interactions are between pentamidine and Phe-168 (-2.904 kcal/mol) and Ser-200 (-2.043 kcal/mol). There are no pi-pi interactions between pentamidine and the residues in the active site of MAO-B.

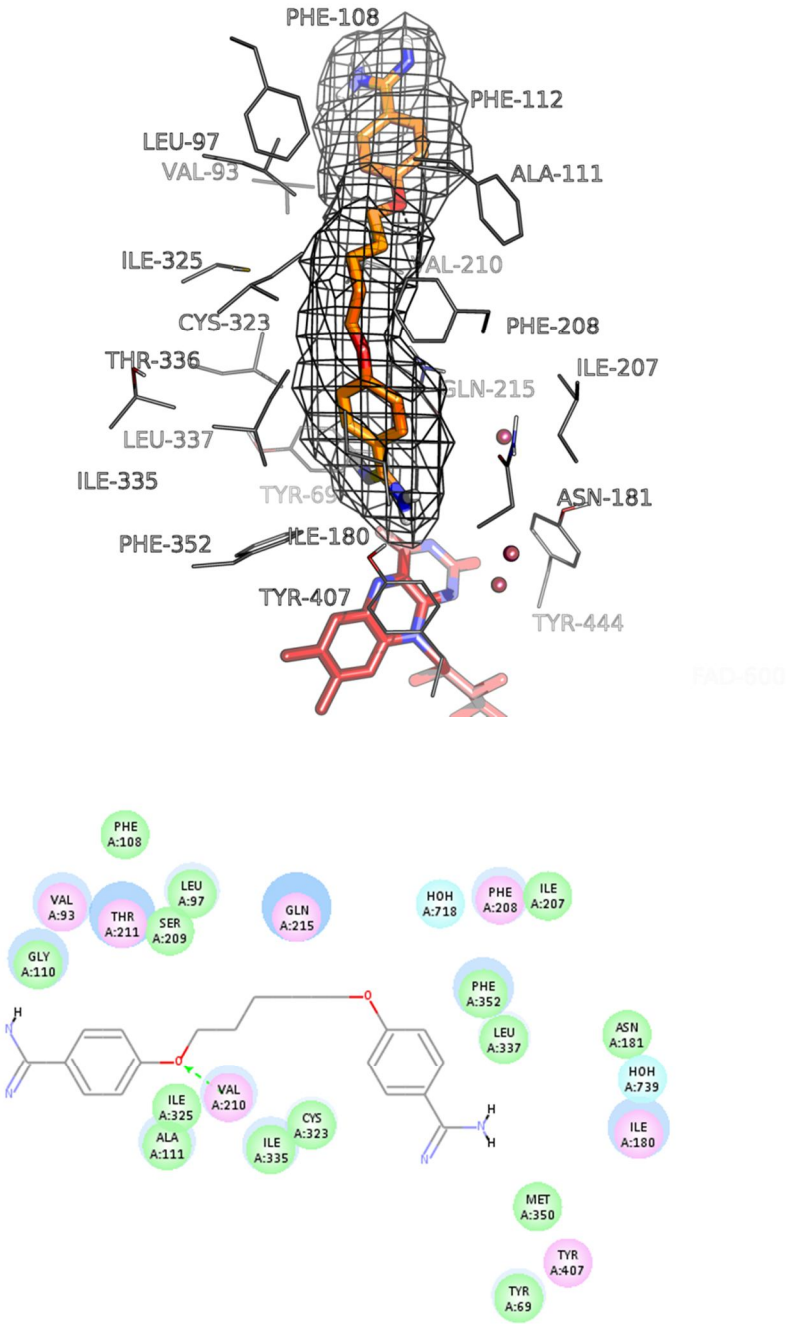

Figure 4.7.46 The docked orientation of pentamidine (in orange) within the MAO-A active site (top). The orientation of the FAD molecule (in red) is also shown. The two-dimensional representation of the binding mode in MAO-A is also given (bottom).

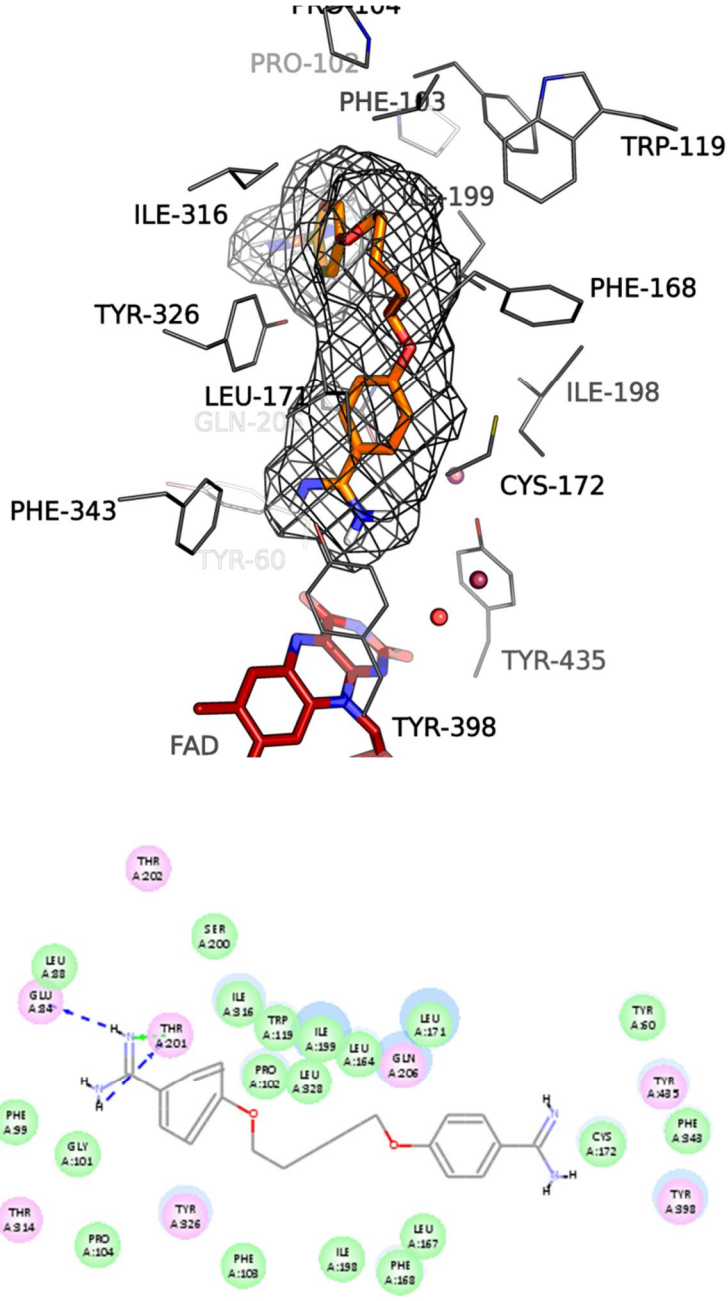

Figure 4.7.47 The docked orientation of pentamidine (in orange) within the MAO-B active site (top). The orientation of the FAD molecule (in red) is also shown. The two-dimensional representation of the binding mode in MAO-B is also given (bottom).

Table 4.7.1 The principal interaction energies of pentamidine with the active site residues and waters of MAO-A. The most productive interactions are shaded.

Name	Forcefield	Total Interaction Energy (kcal/mol)	Total VDW Interaction Energy (kcal/mol)	Total Electrostatic Interaction Energy (kcal/mol)
2Z5X	2Z5X-CHARMm	-52.92033	-43.19524	-9.72509

Interaction Energies			
Residue	**Interaction Energy (kcal/mol)**	**VDW Interaction Energy (kcal/mol)**	**Electrostatic Interaction Energy (kcal/mol)**
A_TYR69	-1.119170	-0.984333	-0.134837
A_VAL93	-2.829740	-2.399240	-0.430498
A_SER94	-0.190286	-0.124484	-0.065802
A_LEU97	-0.466954	-0.483388	0.016434
A_PHE108	-0.579226	-0.462724	-0.116502
A_ARG109	-0.302652	-0.613071	0.310419
A_GLY110	-3.141960	-2.722300	-0.419655
A_ALA111	-2.679170	-2.521530	-0.157645
A_PHE112	-0.395752	-0.539954	0.144202
A_PRO113	-0.165106	-0.126364	-0.038743
A_ILE180	-2.562460	-2.115200	-0.447255
A_ASN181	-0.958148	-0.639141	-0.319007
A_ILE207	-0.707010	-0.596930	-0.110080
A_PHE208	-5.171270	-5.308690	0.137423
A_SER209	-3.142840	-2.944310	-0.198527
A_VAL210	-3.326520	-2.518420	-0.808104
A_THR211	-3.199480	-3.233040	0.033564
A_GLN215	-3.854210	-4.174500	0.320294
A_CYS321	0.034501	-0.075836	0.110337
A_CYS323	-0.895867	-0.877801	-0.018066
A_ILE325	-1.451640	-1.394120	-0.057516
A_ILE335	-2.763440	-2.830970	0.067530
A_THR336	-0.367887	-0.308425	-0.059462
A_LEU337	-1.250850	-1.235190	-0.015656
A_MET350	-0.310747	-0.372845	0.062098
A_PHE352	-1.968870	-1.714940	-0.253934
A_TYR407	-0.802925	-1.433880	0.630955
A_TYR444	-0.509670	-0.219571	-0.290099
A_FAD600	-0.394849	-0.745120	0.350271
A_HOH710	-0.053608	-0.058661	0.005053
A_HOH718	-0.278498	-0.274732	-0.003766
A_HOH739	0.027970	-0.111086	0.139056

Table 4.7.2. The principal interaction energies of pentamidine with the active site residues and waters of MAO-B. The most productive interactions are shaded.

Name	Forcefield	Total Interaction Energy (kcal/mol)	Total VDW Interaction Energy (kcal/mol)	Total Electrostatic Interaction Energy (kcal/mol)
2V5Z	2V5Z-CHARMm	-41.48738	-30.24155	-11.24583

Interaction Energies			
Residue	**Interaction Energy (kcal/mol)**	**VDW Interaction Energy (kcal/mol)**	**Electrostatic Interaction Energy (kcal/mol)**
A_TYR60	-0.533810	-0.664050	0.130240
A_GLU84	-3.093640	0.423141	-3.516780
A_LEU88	0.593593	0.491670	0.101923
A_PHE99	-0.865322	-0.830647	-0.034675
A_GLY101	-0.518761	-0.403469	-0.115292
A_PRO102	1.957910	2.621620	-0.663715
A_PHE103	-1.035100	-1.212700	0.177604
A_PRO104	-0.929095	-0.784005	-0.145090
A_TRP119	-0.951733	-1.066910	0.115177
A_LEU164	-1.064350	-1.113870	0.049525
A_LEU167	-1.394670	-1.565170	0.170501
A_PHE168	-2.904180	-2.654980	-0.249204
A_LEU171	-4.212170	-4.097450	-0.114724
A_CYS172	-1.376860	-1.252620	-0.124236
A_ILE198	-1.656090	-1.819580	0.163493
A_ILE199	-3.205300	-3.325580	0.120279
A_SER200	-2.042920	-1.608930	-0.433993
A_THR201	-0.095196	0.112232	-0.207428
A_THR202	0.052725	-0.251504	0.304229
A_GLN206	-3.113530	-3.376990	0.263462
A_CYS312	-0.159257	-0.049762	-0.109495
A_THR314	-0.855990	-1.493560	0.637570
A_ILE316	0.383724	0.472231	-0.088507
A_TYR326	-1.781240	-1.256660	-0.524578
A_LEU328	-0.435809	-0.603613	0.167804
A_MET341	-0.097065	-0.110729	0.013664
A_PHE343	-1.125230	-0.915398	-0.209827
A_TYR398	-1.508340	-1.906970	0.398633
A_TYR435	-0.726994	-0.713173	-0.013821
A_FAD1502	-0.711865	-0.660643	-0.051222

For further insight, the interactions between pentamidine and the pharmacophore models of MAO-A and MAO-B are also shown. In the pharmacophore model of MAO-A, pentamidine undergoes four hydrophobic interactions. Pentamidine does not undergo any hydrogen bond acceptor or hydrogen bond donor interactions. In the pharmacophore model of MAO-B, pentamidine undergoes interactions with four hydrophobic features but none of the hydrogen bond acceptor or hydrogen bond donor features. This highlights the fact that the hydrophobic interactions between the inhibitor and active sites of the MAOs are important to consider

when constructing pharmacophore models. This finding is in agreement with reports that the active sites of the MAOs are, for the most part, hydrophobic spaces.

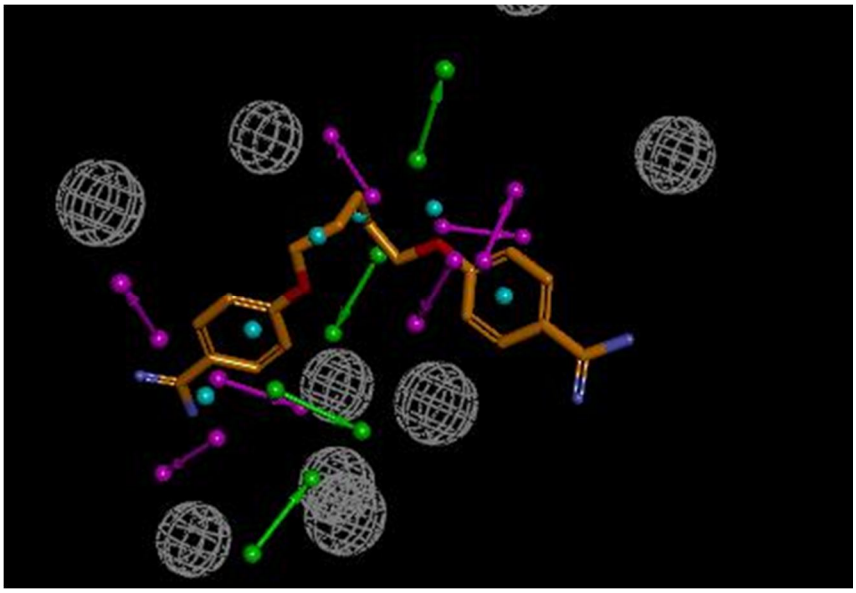

Figure 4.7.48 Pentamidine mapped to the pharmacophore model of MAO-A.

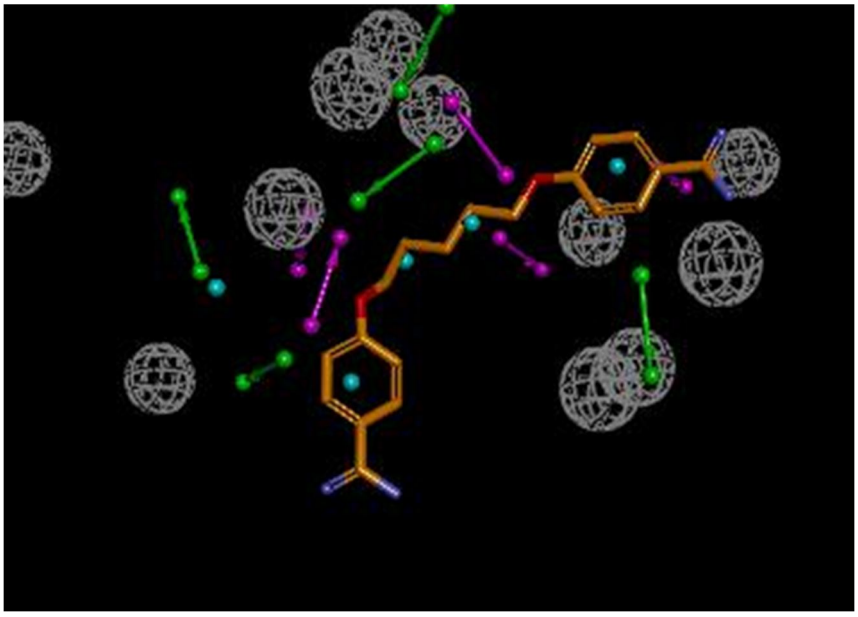

Figure 4.7.49 Pentamidine mapped to the pharmacophore model of MAO-B.

The MAO inhibitory properties of isethionate salt was examined in order to determine whether the MAO inhibitory properties of pentamidine isethionate may possibly be mediated by the isethionic counter ion used for the salt form of pentamidine. The results are given below and show that the isethionate salt does not inhibit either MAO-A or MAO-B and

therefore pentamidine is responsible for the MAO inhibition of the pentamidine isethionate complex.

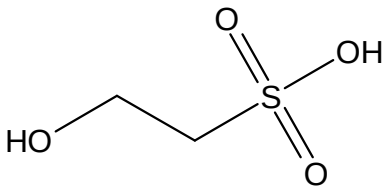

Figure 4.7.50 The structure of isethionic acid

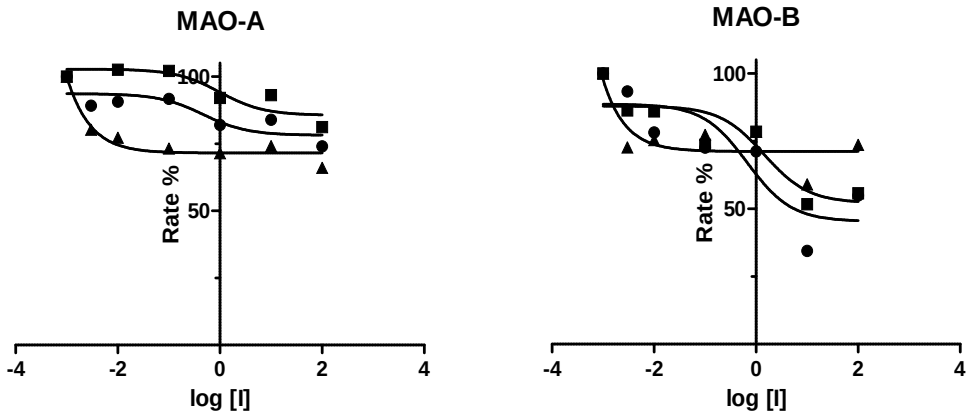

Figure 4.7.51 The recombinant human MAO-A (left) and MAO-B (right) catalyzed oxidation of kynuramine in the presence of various concentrations of isethionic acid (expressed in µM). The concentration-response curves were constructed in triplicate from the initial rates of kynuramine oxidation versus the logarithm of the concentration of the isethionic acid. The rates are expressed as the percentage of the catalytic rate recorded in the absence of inhibitor.

4.7.22 **Phenformin:**

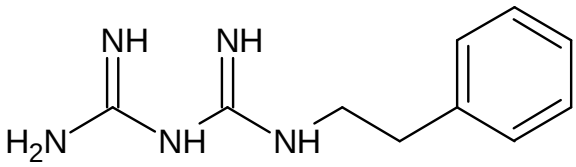

Figure 4.7.52 The structure of phenformin.

Phenformin is an oral antidiabetic drug of the biguanide class. Cubría *et al.* (1991) have evaluated the structurally related compounds phenformin (a biguanide) and pentamidine (an amidine) as potential inhibitors of porcine kidney diamine oxidase. They found that pentamidine was a more potent inhibitor of diamine oxidase than phenformin, but that both

were non-competitive inhibitors (with K_i values of 3 µM for pentamidine and 4 mM for phenformin). This study examined the human MAO inhibition properties of phenformin. The results show that phenformin is a selective inhibitor of MAO-A, but not of MAO-B. The inhibition of MAO-B by phenformin was evaluated up to a maximal concentration of 100 µM, while and the inhibition of MAO-A by phenformin was evaluated up to a maximal concentration of 1 mM. The IC_{50} value for the inhibition of MAO-A by phenformin was found to be 40.5 ±4.36 µM. The concentration-response curves of the MAO-A and MAO-B catalytic rates in the presence of increasing concentrations of phenformin are given below.

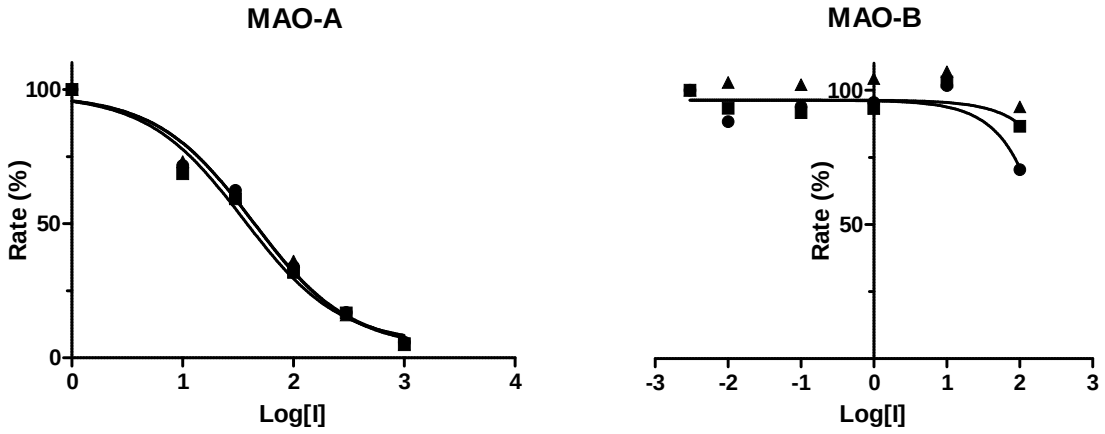

Figure 4.7.53 The recombinant human MAO-A (left) and MAO-B (right) catalyzed oxidation of kynuramine in the presence of various concentrations of phenformin (expressed in µM). The concentration-response curves were constructed in triplicate from the initial rates of kynuramine oxidation versus the logarithm of the concentration of phenformin. The rates are expressed as the percentage of the catalytic rate recorded in the absence of inhibitor.

The reversibility of the interaction of phenformin with MAO-A was further investigated by evaluating the recovery of the enzymatic activity after dilution of the enzyme-inhibitor complexes. For this purpose, MAO-A was preincubated with phenformin at concentrations of 10 × IC_{50} and 100 × IC_{50} for 30 min. The reactions were subsequently diluted 100-fold to 0.1 × IC_{50} and 1 × IC_{50}, respectively. The results are given in figure 4.7.54 and show that phenformin is a reversible inhibitor of MAO because enzyme activity is recovered after dilution of the inhibitor. After dilution of the phenformin complex to 0.1 × IC_{50} and 1 × IC_{50}, the MAO-A catalytic activities are recovered to 95% and 56%, respectively, of the control value. For comparison, after similar treatment of MAO-A with the irreversible inhibitor pargyline (at 10 × IC_{50}) and dilution of the resulting complexes to 0.1 × IC_{50}, MAO-A activity is not recovered (3.4% of control). The recovery of the MAO-B catalytic activity after dilution was not evaluated because phenformin is a selective MAO-A inhibitor. It may thus be concluded that phenformin interacts reversibly with MAO-A. For reversible enzyme inhibition,

the enzyme activities are expected to recover to levels of approximately 90% and 50%, respectively, after dilution of the inhibitor to 0.1 × IC_{50} and 1 × IC_{50}.

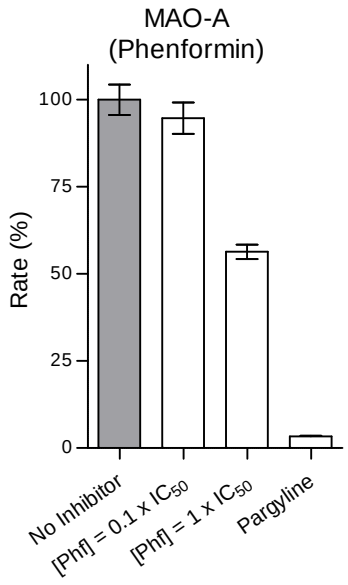

Figure 4.7.54 Reversibility of inhibition of MAO-A by phenformin. The enzyme was preincubated with the test inhibitor at 10 × IC_{50} and 100 × IC_{50} for 30 min and then diluted to 0.1 × IC_{50} and 1 × IC_{50}, respectively. As controls, MAO-A was also preincubated with pargyline at 10 × IC_{50} and subsequently diluted to 0.1 × IC_{50}. The residual enzyme activities were subsequently measured.

The reversibility of the MAO-A inhibition by phenformin was also investigated by measuring the recovery of enzyme activity after dialysis of enzyme-inhibitor mixtures (Harfenist *et al*., 1996). MAO-A and phenformin, at a concentration of 4 × IC_{50}, were preincubated for a period of 15 min and subsequently dialyzed for 24 h. The results, given in Fig. 4.7.55, show that the MAO-A inhibition by phenformin is completely reversed after 24 h of dialysis with the MAO-A activity recovering to a level of 110% of the control value. In contrast, the MAO-A activity in undialyzed mixtures of MAO-A with phenformin is 36% of the control value. This behaviour is consistent with a reversible interaction between MAO-A and phenformin. For comparison, after similar preincubation and dialysis of MAO-A with the irreversible inhibitor, pargyline, the enzyme activity is not recovered. After dialysis of a MAO-A–pargyline mixture, the residual enzyme activity is only 1.7% of the control value.

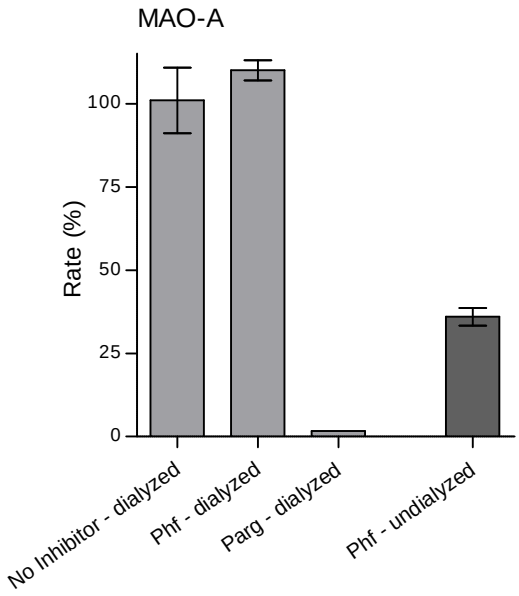

Figure 4.7.55 Reversibility of inhibition of MAO-A by phenformin. MAO-A and phenformin, at an inhibitor concentration of 4 × IC_{50}, were preincubated together, dialyzed and the residual MAO activity was subsequently measured (Phf–dialyzed). For comparison, MAO-A was similarly preincubated in the absence (No inhibitor–dialyzed) and presence of the irreversible inhibitor, pargyline (Parg–dialyzed), and dialyzed. The residual MAO activities of undialyzed mixtures (Phf–undialyzed) of MAO-A with phenformin is also shown.

To provide additional insight, the binding mode of phenformin within the active site cavity of MAO-A was examined. The molecular docking simulation was carried out according to the protocol given in Chapter 3. The results are given in figure 4.7.56 and table 4.7.3. As seen from the two dimensional representation of the binding of phenformin in the active site of MAO-A, phenformin undergoes hydrogen bond donor interactions with Gly-214 (-0.812 kcal/mol), Gln-215 (-7.193 kcal/mol) and Tyr-407 (-2.139 kcal/mol). As can be seen from the cyan sphere, the interaction with Gln-215 is also a hydrophobic interaction and the large negative value indicates that it is an important interaction. Other hydrophobic interactions are with Tyr-69 (-2.160 kcal/mol), Ile-180 (-0.084 kcal/mol), Phe-208 (-2.696 kcal/mol), Ile-335 (-2.096 kcal/mol), Phe-352 (-1.659 kcal/mol) and Tyr-444 (-1.378 kcal/mol).

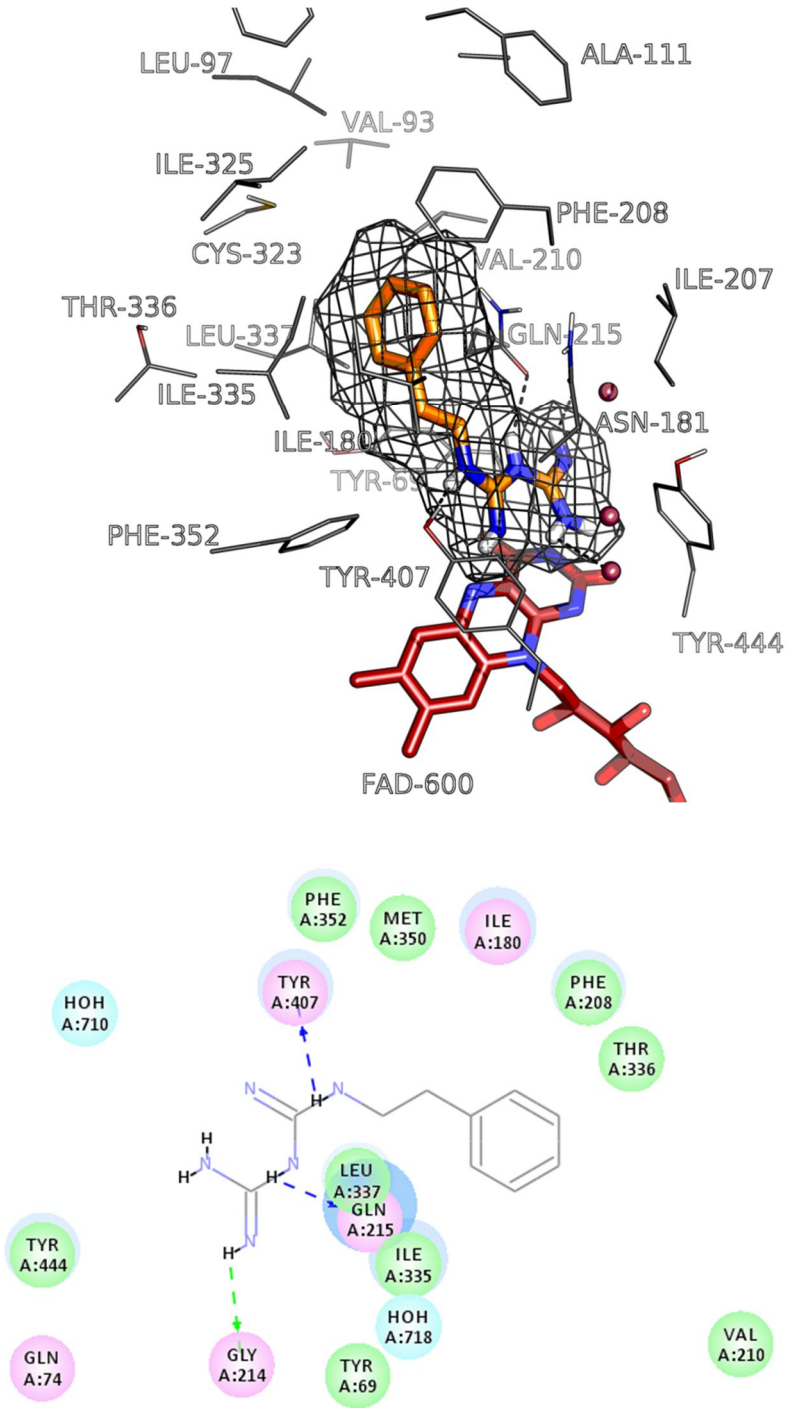

Figure 4.7.56 The docked orientation of phenformin (in orange) within the MAO-A active site (top). The orientation of the FAD molecule (in red) is also shown as a reference point. The two-dimensional representation of the binding mode in MAO-A is also given (bottom).

Table 4.7.3 The principal interaction energies of phenformin with the active site residues and waters of MAO-A. The most productive interactions are shaded.

Name	Forcefield	Total Interaction Energy (kcal/mol)	Total VDW Interaction Energy (kcal/mol)	Total Electrostatic Interaction Energy (kcal/mol)
2Z5X	2Z5X-CHARMm	-36.82920	-21.50191	-15.32728

Interaction Energies			
Residue	**Interaction Energy (kcal/mol)**	**VDW Interaction Energy (kcal/mol)**	**Electrostatic Interaction Energy (kcal/mol)**
A_TYR69	-2.160230	-2.140320	-0.019909
A_VAL70	-0.156275	-0.180379	0.024104
A_GLN74	-0.415634	-0.223255	-0.192379
A_LEU97	-0.109013	-0.082914	-0.026100
A_ILE180	-0.084351	0.239049	-0.323400
A_ASN181	-0.754864	-0.582086	-0.172778
A_ILE207	-0.618734	-0.521474	-0.097260
A_PHE208	-2.696450	-2.243000	-0.453452
A_SER209	-0.539519	-0.338158	-0.201361
A_VAL210	-0.426194	-0.495043	0.068849
A_GLY214	-0.811638	-0.882388	0.070750
A_GLN215	-7.192770	-5.288530	-1.904240
A_CYS323	-0.134481	-0.233493	0.099012
A_ILE325	-0.281689	-0.275598	-0.006091
A_ILE335	-2.095690	-2.085520	-0.010172
A_THR336	-0.551785	-0.450552	-0.101233
A_LEU337	-1.530190	-1.584330	0.054143
A_MET350	-0.586518	-0.545600	-0.040918
A_PHE352	-1.659250	-1.796320	0.137065
A_LEU354	0.069906	-0.126847	0.196753
A_TYR407	-2.139310	-1.410510	-0.728796
A_TRP441	-0.346809	-0.261796	-0.085013
A_GLY443	-0.183077	-0.106402	-0.076675
A_TYR444	-1.377680	-1.233440	-0.144244
A_MET445	-0.254893	-0.166754	-0.088139
A_FAD600	-1.295100	0.897360	-2.192460
A_HOH710	-0.769264	-0.487447	-0.281817
A_HOH718	-0.151101	-0.921431	0.770330
A_HOH739	-0.237732	-0.356060	0.118328

For further insight, the interactions of phenformin with the pharmacophore model of MAO-A are also shown. In the pharmacophore model of MAO-A, phenformin undergoes interactions with two hydrogen bond donor features and two hydrophobic features. Phenformin does not undergo interactions with any hydrogen bond acceptor features.

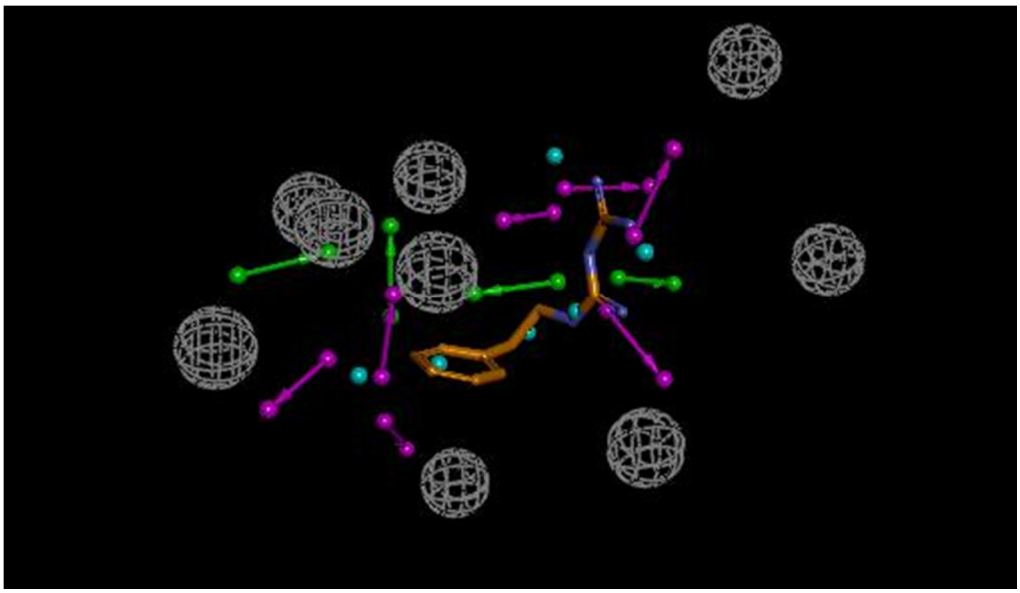

Figure 4.7.57 Phenformin mapped to the pharmacophore model of MAO-A.

4.7.23 **Metoprolol:**

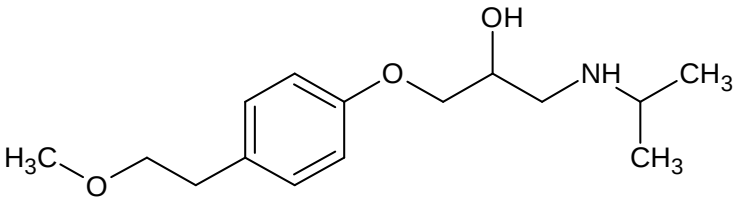

Figure 4.7.58 The structure of metoprolol.

Metoprolol is a β1-selective adrenergic antagonist that is used in cardiovascular conditions such as hypertension. The results show that metoprolol is an inhibitor of MAO-B, but not of MAO-A. The maximum tested concentration for MAO-A was 100 µM, while for MAO-B it was 1 mM. The IC_{50} value for the inhibition of MAO-B by metoprolol was found to be 94.3 ±15.2 µM. The concentration-response curves of the MAO-A and MAO-B catalytic activities in the presence of increasing concentrations of metoprolol are given below.

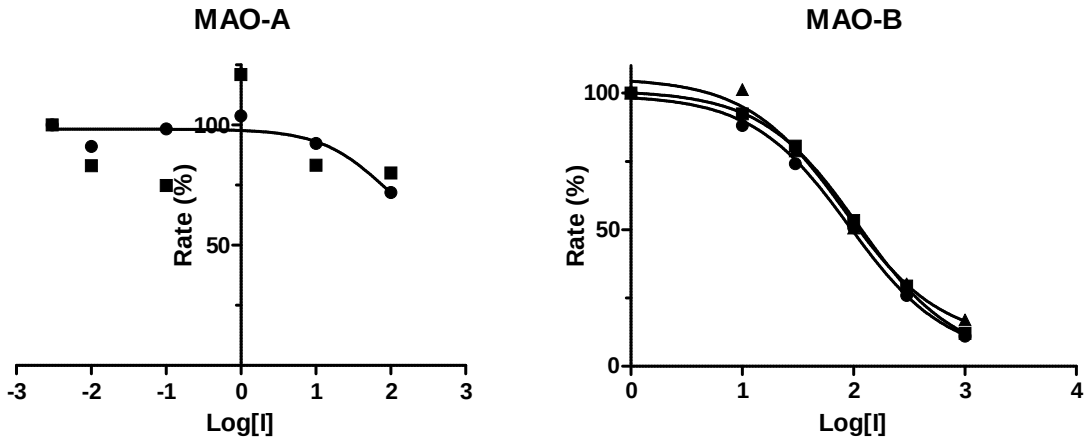

Figure 4.7.59 The recombinant human MAO-A (left) and MAO-B (right) catalyzed oxidation of kynuramine in the presence of various concentrations of metoprolol (expressed in µM). The concentration-response curves were constructed in triplicate from the initial rates of kynuramine oxidation versus the logarithm of the concentration of metoprolol. The rates are expressed as the percentage of the catalytic rate recorded in the absence of inhibitor.

4.7.24 Fluoxetine:

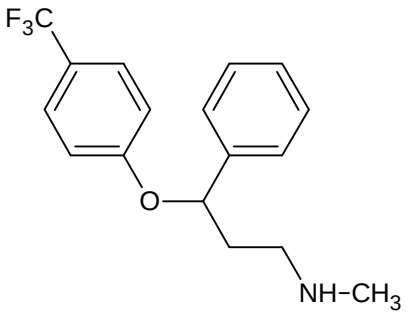

Figure 4.7.60 The structure of fluoxetine.

Fluoxetine is an antidepressant of the selective serotonin reuptake inhibitor class. Previous studies by Mukherjee & Yang (1999), have found that fluoxetine inhibits both MAO-A and MAO-B in rat brains with a binding affinity of 36.5 µM for MAO-A. Our studies determined the IC_{50} values for the inhibition of MAO-A and MAO-B using the human enzymes. The maximal concentration used for the IC_{50} determination was 8 mM for MAO-A and 3 mM for MAO-B. The IC_{50} values for the inhibition of MAO-A and MAO-B by fluoxetine were found to be 133 ± 9.15 µM and 41.7 ± 21.1 µM, respectively.

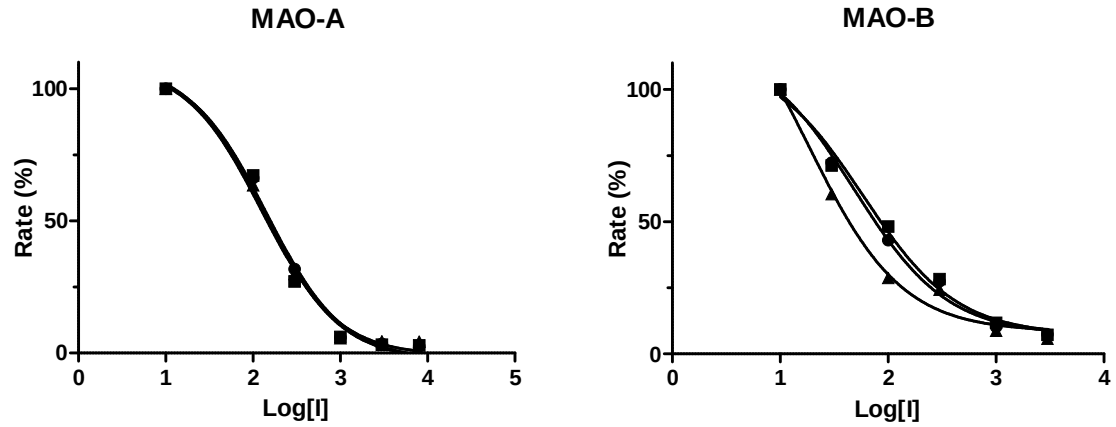

Figure 4.7.61 The recombinant human MAO-A (left) and MAO-B (right) catalyzed oxidation of kynuramine in the presence of various concentrations of fluoxetine (expressed in µM). The concentration-response curves were constructed in triplicate from the initial rates of kynuramine oxidation versus the logarithm of the concentration of fluoxetine. The rates are expressed as the percentage of the catalytic rate recorded in the absence of inhibitor.

4.7.25 Terfenadine:

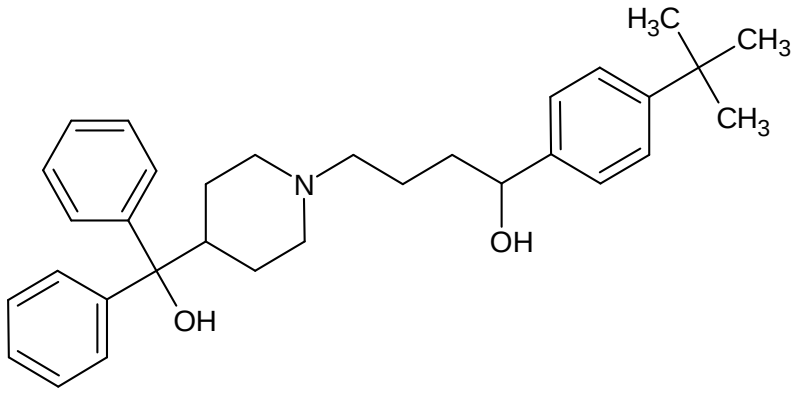

Figure 4.7.62 The structure of terfenadine.

Terfenadine is a prodrug of the second generation antihistamine fexofenadine. The results show that terfenadine is an inhibitor of both MAO-A and MAO-B. Due to solubility problems it could not be evaluated at concentrations above 100 µM and complete suppression of MAO-A and MAO-B could therefore not be achieved. The IC_{50} values for the inhibition of MAO-A and MAO-B by terfenadine were found to be 112 ± 36.7 µM and 8.41 ± 3.70 µM, respectively. The concentration-response curves of the MAO-A and MAO-B catalytic activities in the presence of increasing concentrations of terfenadine are given below.

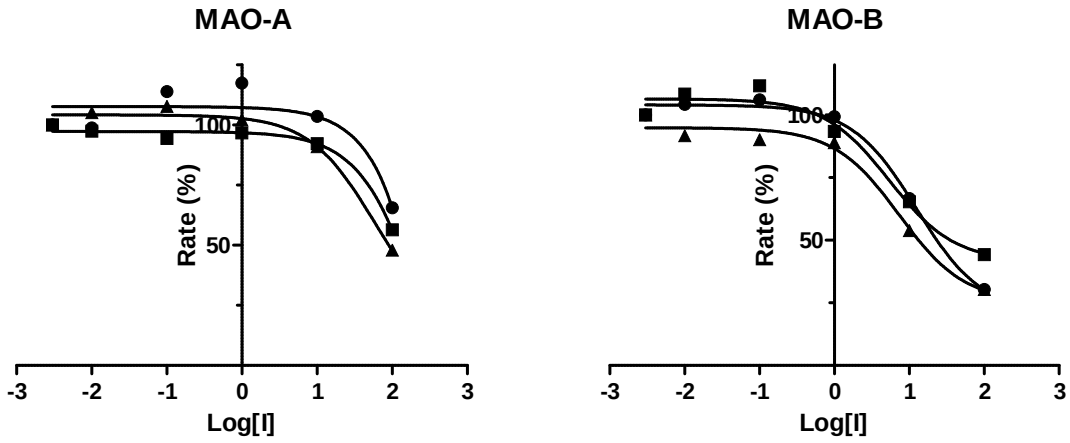

Figure 4.7.63 The recombinant human MAO-A (left) and MAO-B (right) catalyzed oxidation of kynuramine in the presence of various concentrations of terfenadine (expressed in µM). The concentration-response curves were constructed in triplicate from the initial rates of kynuramine oxidation versus the logarithm of the concentration of terfenadine. The rates are expressed as the percentage of the catalytic rate recorded in the absence of inhibitor.

4.7.26 Lansoprazole:

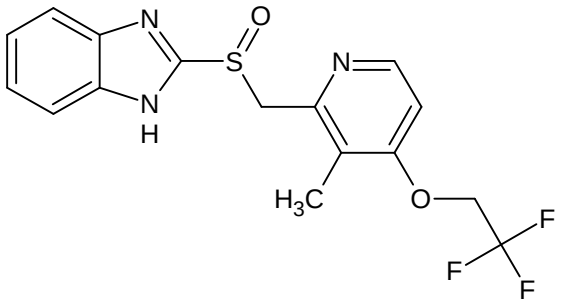

Figure 4.7.64 The structure of lansoprazole.

Lansoprazole is a proton pump inhibitor that is used to suppress the formation of gastric acid formation in the treatment of conditions such as peptic ulcer disease and gastro-oesophageal reflux disease. The results show that lansoprazole is a relatively good inhibitor of MAO-A with an IC_{50} value of 31.0 ±18.6 µM, and a weak inhibitor of MAO-B for which complete suppression could not be obtained at the maximum tested concentration of 100 µM. Lansoprazole could not be evaluated at higher concentrations due to limited aqueous solubility. The concentration-response curves of the MAO-A and MAO-B catalytic activities in the presence of increasing concentrations of lansoprazole are given below.

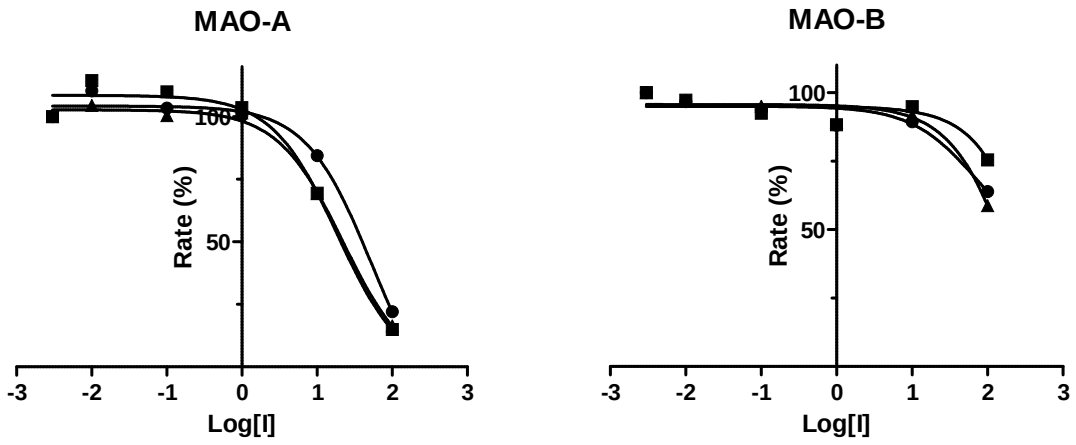

Figure 4.7.65 The recombinant human MAO-A (left) and MAO-B (right) catalyzed oxidation of kynuramine in the presence of various concentrations of lansoprazole (expressed in µM). The concentration-response curves were constructed in triplicate from the initial rates of kynuramine oxidation versus the logarithm of the concentration of lansoprazole. The rates are expressed as the percentage of the catalytic rate recorded in the absence of inhibitor.

4.8 Results of the MAO inhibition studies with known MAO inhibitors:

The MAO inhibition potencies of the active drugs were compared to the IC_{50} values of known inhibitors previously determined by our laboratory (Petzer *et al.,* 2013). The following inhibitors were selected:

- MAO-A inhibitor: Toloxatone
- MAO-B inhibitor: Lazabemide

4.8.1 Toloxatone:

The results of the MAO-A inhibition studies previously done by this laboratory show that toloxatone inhibits MAO-A with an IC_{50} value of 3.92 ± 0.015 µM (Petzer *et al.*, 2013)

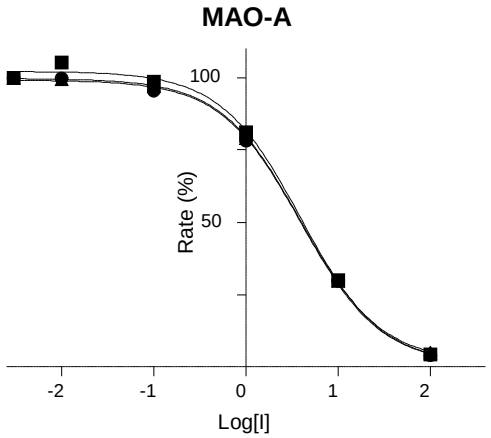

Figure 4.8.1 The recombinant human MAO-A catalyzed oxidation of kynuramine in the presence of various concentrations of toloxatone (expressed in µM). The concentration-response curves were constructed from the initial rates of kynuramine oxidation versus the logarithm of the concentration of toloxatone.

4.8.2 Lazabemide:

The results of previous MAO-B inhibition studies done by this laboratory show that lazabemide inhibits MAO-B with an IC_{50} value of 0.091 ± 0.015 µM (Petzer *et al.*, 2013).

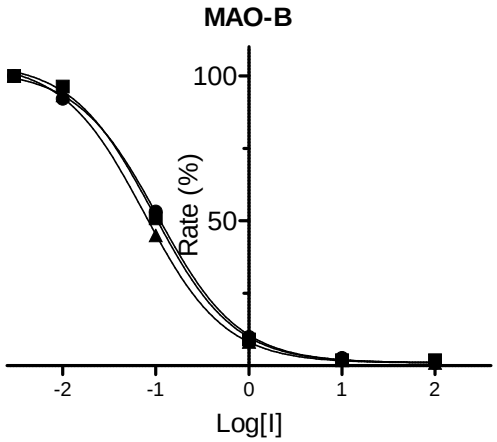

Figure 4.8.2 The recombinant human MAO-B catalyzed oxidation of kynuramine in the presence of various concentrations of lazabemide (expressed in µM). The concentration-response curves were constructed from the initial rates of kynuramine oxidation versus the logarithm of the concentration of lazabemide.

4.9 Summary:

In this chapter, 26 drugs which mapped to the pharmacophore models were evaluated as *in vitro* inhibitors of human MAO-A and MAO-B. Of these, 20 drugs had little or no MAO inhibitory activity at the maximum tested concentration of 100 µM. These compounds may have the required features to map to the pharmacophore models, but they are not strong inhibitors *in vitro.* This suggests that the approach to pharmacophore model development and screening may have to be modified. For example, using shape constraints instead of exclusion constraints and adding certain required features for compounds to be considered hits may improve the predictive value of the models. Furthermore, the MAO enzymes are inhibited by a large number of compounds and a wide variety of drugs may map to the pharmacophore models without being significant inhibitors *in vitro.*

The *in vitro* results show that 6 of the compounds that mapped to the pharmacophore models of MAO-A and/or MAO-B, namely: pentamidine, phenformin, metoprolol, fluoxetine, terfenadine and lansoprazole were relatively good inhibitors of MAO-A and/or MAO-B. Of these, pentamidine and phenformin were selected for further analysis. Pentamidine (an amidine) and phenformin (a biguanide) are both guanidine derivatives and therefore share a degree of structural similarity. Pentamidine was a more potent inhibitor of both MAO-A and MAO-B than phenformin, which only inhibited MAO-A. Further analysis showed that they were both reversible inhibitors of MAO. Pentamidine and phenformin both have severe adverse effects and are therefore not suited for repurposing as MAO inhibitors, but as shown in the next chapter, the knowledge of their MAO inhibitory activities should be considered when evaluating the toxicological profiles of these drugs. Since pentamidine is used in severely ill patients, where the benefits outweigh the risk, this knowledge is especially crucial. Due to the similarity of the key functional groups of both pentamidine and phenformin, this research has shown that the amidine, and to a lesser extent the biguanide, functional groups may be used as new leads in the future design of new MAO inhibitors. Since the guanidine derivatives have also been postulated to inhibit the nitric oxide synthases (NOS), future inhibitors based on these functional groups may be bifunctional in their mode of action (Xian *et al.*, 2001). The MAO inhibition results obtained with pentamidine and phenformin will be further discussed in the following chapter.